ECONOMIC GEOLOGY

AND THE

BULLETIN OF THE SOCIETY OF ECONOMIC GEOLOGISTS

VOL. 85 JUNE–JULY, 1990 NO. 4

Carbonate Petrography, Kerogen Distribution, and Carbon and Oxygen Isotope Variations in an Early Proterozoic Transition from Limestone to Iron-Formation Deposition, Transvaal Supergroup, South Africa

NICOLAS J. BEUKES,

Department of Geology, Rand Afrikaans University, Johannesburg 2000, South Africa

CORNELIS KLEIN,

Department of Geology, University of New Mexico, Albuquerque, New Mexico 87131

ALAN J. KAUFMAN*, AND J. M. HAYES

Biogeochemical Laboratories, Geology Building, Indiana University, Bloomington, Indiana 47405-5101

Abstract

The transition zone comprises Campbellrand microbialaminated (replacing "cryptalgalaminate") limestone and shale, with minor dolomite, conformably overlain by the Kuruman Iron Formation of which the basal part is characterized by siderite-rich microbanded iron-formation with minor magnetite and some hematite-containing units. The iron-formation contains subordinate intraclastic and microbialaminated siderite mesobands and was deposited in deeper water than the limestones. The sequence is virtually unaltered with diagenetic mineral assemblages reflecting a temperature interval of about 110° to 170°C and pressures of 2 kbars.

Carbonate minerals in the different rock types are represented by primary micritic precipitates (now recrystallized to microsparite), early precompactional sparry cements and concretions, deep burial limpid euhedral sparites, and spar cements precipitated from metamorphic fluids in close contact with diabase sills. Paragenetic pathways of the carbonate minerals are broadly similar in all lithofacies with kerogen intimately associated with them. Kerogen occurs as pigmentation in carbonate crystals, as reworked organic detritus in clastic-textured carbonate units, and as segregations of kerogen pigment around late diagenetic carbonate crystals. Locally kerogen may also be replaced by carbonate spar. Carbon isotope compositions of the carbonate minerals and kerogen are dependent on their mode of occurrence and on the composition of the dominant carbonate species in a specific lithofacies.

Integration of sedimentary, petrographic, geochemical, and isotopic results makes it possible to distinguish between depositional, early diagenetic, deep burial, and metamorphic effects on the isotopic compositions of the carbonate minerals and the kerogen in the sequence. Major conclusions are that deep burial thermal decarboxylation led to ^{13}C depletion in euhedral ferroan sparites and ^{13}C enrichment in kerogen (organic carbon). Metamorphic sparites are most depleted in ^{13}C. Carbonates in oxide-rich iron-formations are more depleted in ^{13}C than those in siderite-rich iron-formation whereas the kerogens in oxide banded iron-formations (BIF) are more enriched. This implies that the siderite-rich iron-formations were not derived from oxide-rich iron-formation through reduction of ferric iron by organic matter. Organic matter oxidation by ferric iron did, however, decrease the abundance of kerogen in oxide-rich iron-formation and led to the formation of isotopically very light sparry carbonates.

Siderite and calcmicrosparite both represent recrystallized primary micritic precipitates but differ in their ^{13}C composition, with the siderites depleted in ^{13}C by 4.6 per mil on average relative to calcmicrosparite. This means that the siderites were precipitated from water with dissolved inorganic carbon depleted in ^{13}C by about 9 per mil relative to that from which the limestones precipitated. This implies an ocean system stratified with regard to total carbonate, with the deeper water, from which siderite-rich iron-formation formed, depleted in ^{13}C. Iron-

* Present address: Department of Earth and Planetary Sciences, Harvard University, Cambridge, Massachusetts 02138.

0361-0128/90/1063/663-28$3.00

formations were deposited in areas of very low organic matter supply. Depletion of ^{13}C may, therefore, derive not from degradation of organic matter but from hydrothermal activity, a conclusion which is supported by ^{18}O composition of the carbonate minerals and trace element and rare earth element (REE) compositions of the iron-formations.

Introduction

IRON-RICH carbonate minerals (siderite and ankerite) in early Proterozoic iron-formations are depleted in ^{13}C by 5 to 15 per mil relative to most dolomites and limestones (Becker and Clayton, 1972; Perry and Tan, 1972; Perry et al., 1973; Perry and Ahmad, 1981; Baur et al., 1985; Kaufman et al., in press). Organic carbon in iron-formations, however, is generally enriched in ^{13}C relative to that in associated carbonate sequences (Baur et al., 1985). These isotopic characteristics of iron-formations have been attributed to special conditions of formation such as deposition in an enclosed basin (Becker and Clayton, 1972), biological production of ^{13}C-depleted CO_2 below the sediment water interface (Baur et al., 1985), and diagenetic to metamorphic reactions between hematite and organic carbon (Perry et al., 1973; Perry and Ahmad, 1981). These interpretations have been based on the hypothesis that the distribution and isotopic composition of total dissolved carbon in Proterozoic open-marine systems were similar to those of the present-day (Becker and Clayton, 1972), as based on the distribution of ^{13}C in coeval limestones and dolomites (Schidlowski et al., 1983). The assumption that carbonate grains in ancient limestones and dolomites reflect the isotopic composition of total carbonate in ancient open-ocean systems, but that those in iron-formations do not, has not been carefully tested. Detailed studies of areas where iron-formation is closely related to or interbedded with limestone-dolomite have not been made; indeed, relationships between different lithofacies have been largely ignored. Furthermore, there is a lack of information on the paragenesis of the carbonate minerals and the mode of occurrence and abundance of organic matter in iron-formations and related lithofacies.

The Griqualand West area of the Transvaal basin in South Africa offers a unique opportunity to study the relationships between the deposition of limestone and iron-formation. The stratigraphic sequence includes the transition from stromatolitic carbonates of the Gamohaan Formation of the Campbellrand Subgroup to conformably overlying Kuruman Iron Formation (Fig. 1), which is composed mainly of microbanded iron-formation (Beukes, 1984). Klein and Beukes (1989) report in detail on inorganic geochemical and sedimentological aspects of this transition zone based on intersections in three deep diamond drill cores from Derby (core DI-1), Whitebank (core WB-98), and Pomfret (core AD-5) (Fig. 2). Here we report on the relationships between carbonate mineral paragenesis, kerogen abundance, and isotopic compositions of carbon and oxygen for the same drill core samples. Our purpose is to explore the significance of whole-rock carbon isotope compositions of iron-formations relative to those of limestones and dolomites. Such an integrated approach may also help clarify whether ^{18}O values in low-grade metamorphic iron-formations have synsedimentary environmental significance or whether they are the result of post-depositional open-system isotopic exchange (Gregory, 1986).

The various rock types in the Campbellrand-Kuruman transition sequence are especially well suited for these studies because they are generally only weakly deformed. The drill cores are situated on the Kaapvaal craton and the strata dip gently at less than

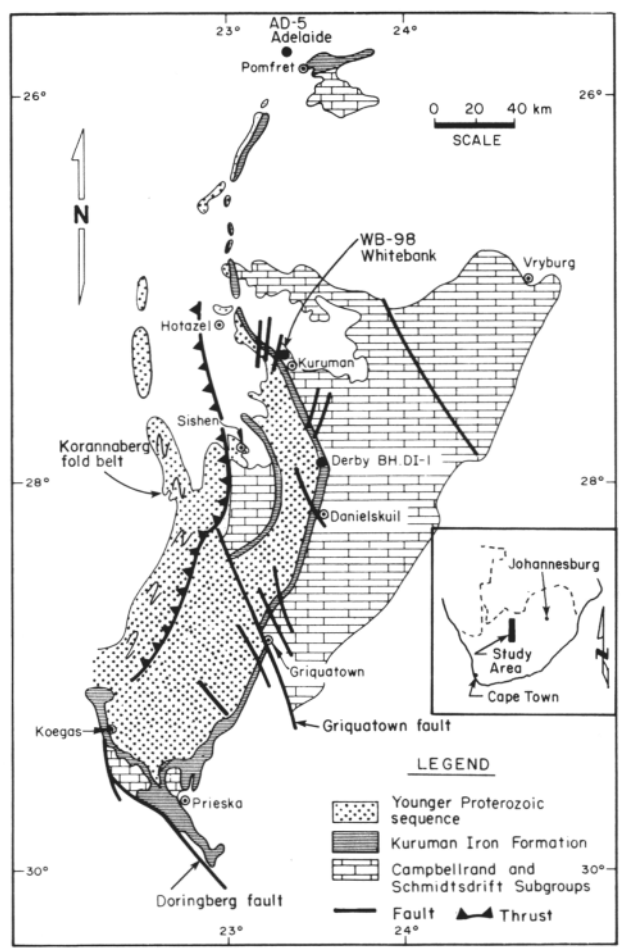

FIG. 1. Geologic map showing the distribution of the Kuruman Iron Formation and the location of boreholes Derby DI-1, Whitebank WB-98, and Pomfret AD-5 (after Klein and Beukes, 1989).

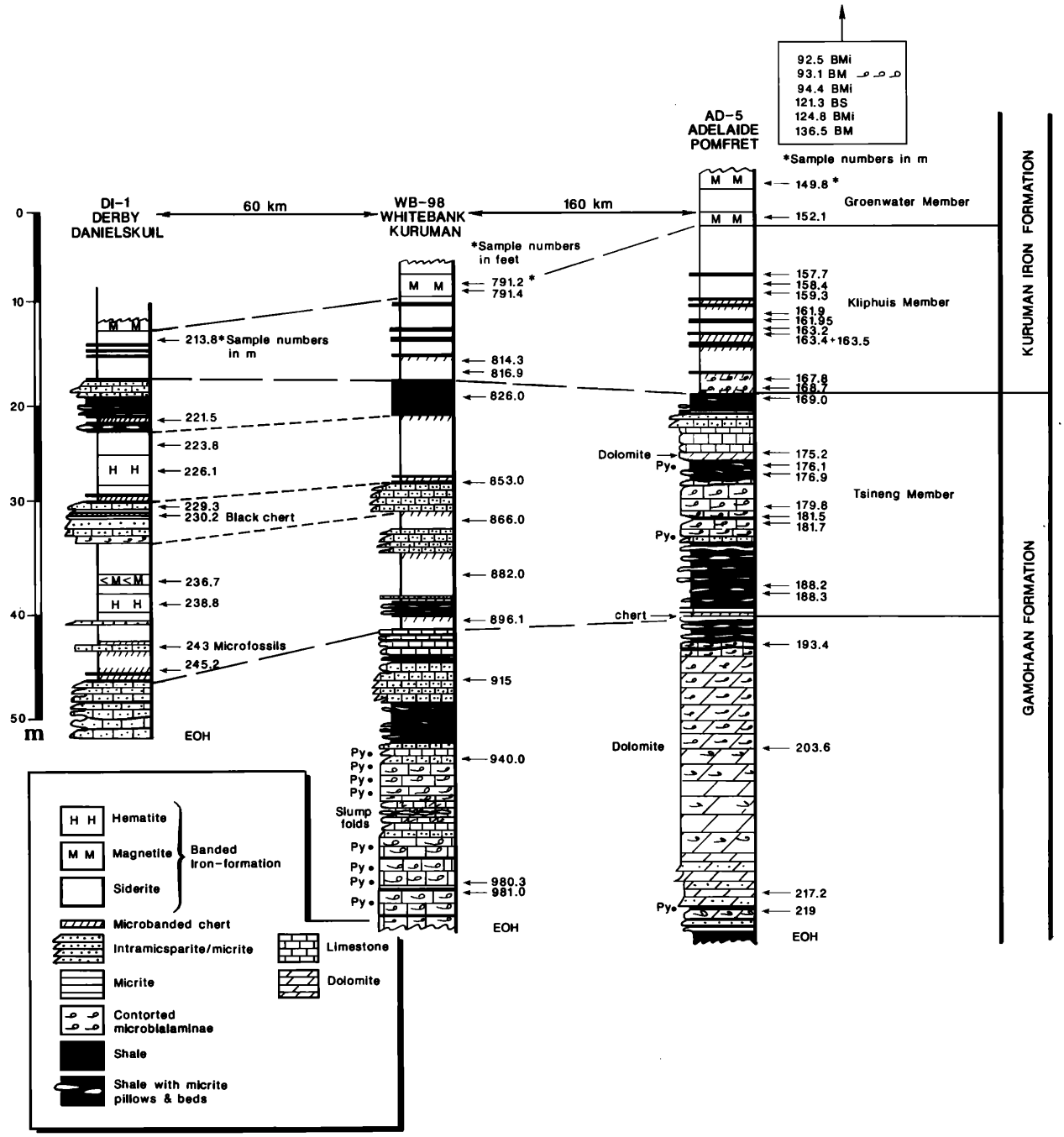

FIG. 2. Correlation of stratigraphic units in the three boreholes DI-1, WB-98, and AD-5. All samples studied are located either in meters, or in feet, as follows: B = BIF = banded iron-formations; H = hematite; M = magnetite; Mi = minnesotaite rich; S = siderite rich (after Klein and Beukes, 1989).

5° W (Fig. 1). Maximum regional diagenetic temperatures are estimated to have been on the order of 110° to 170°C at pressures about 2 kbars or less (Miyano and Beukes, 1984). The best available age bracket for the sequence is between 2,357 ± 53 and 2,239 ± 90 Ma (Walraven et al., 1990). However, some uncertainties are involved in the interpretation of these ages, and the deposition of the Campbellrand carbonate sequence may have started as much as 2,500 Ma ago (Beukes, 1987).

Indications are that the carbonates and iron-formations were deposited under passive platformal tec-

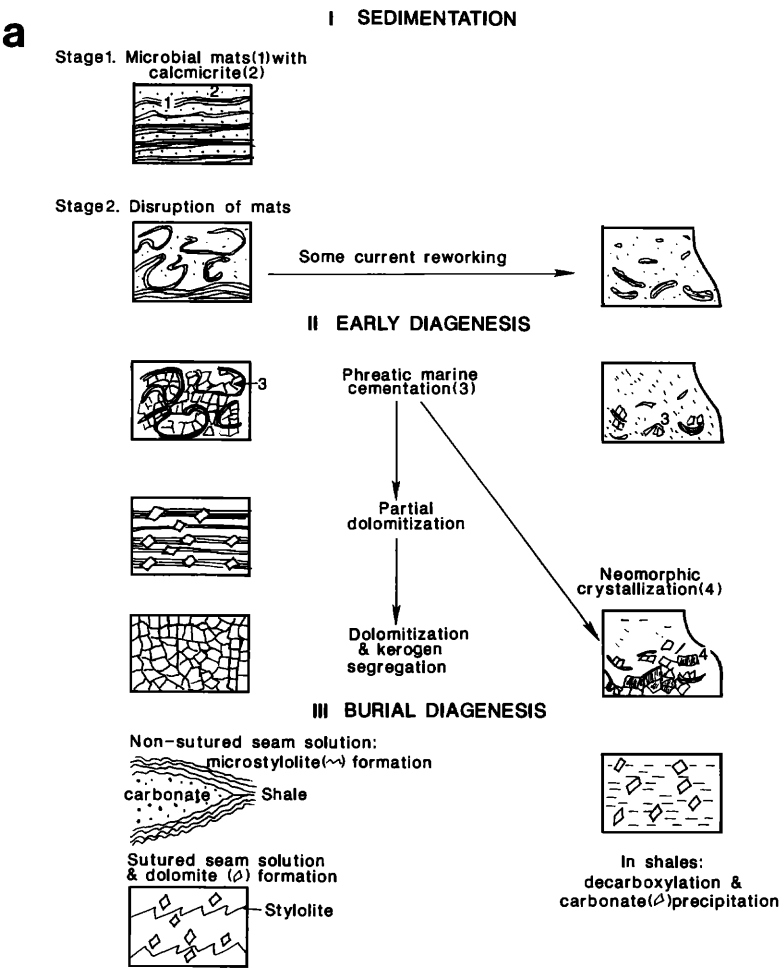

FIG. 3. Major petrographic features of the limestones, dolomites, and siderite-rich iron-formations.

tonic conditions over very extensive areas of the Kaapvaal craton. During deposition of the Kuruman Iron Formation, virtually the whole of the craton must have been submerged, allowing for total absence of siliciclastic input (Beukes, 1983). The basin deepened toward the western and southwestern edge of the craton into what may have been a back-arc type setting, allowing for minor amounts of tuffaceous material to reach the platform from an external volcanic source situated off the craton to the west (Beukes, 1983, 1987). This situation may have persisted until deposition of the Kalahari manganese deposits near the top of the Transvaal Sequence in Griqualand West (Nel et al., 1986). Compressional tectonics with related thrusting only took place much later in the history of the sequence, following deposition of late early-Proterozoic Olifantshoek red beds (Stowe, 1986; Beukes and Smit, 1987). It is thus highly unlikely that the iron-formations of the Transvaal Sequence were deposited in linear foreland basins similar to those that may characterize the deposition of granular iron-formation units of the Canadian Shield according to Hoffman (1987).

Stratigraphy and Sample Selection

The Campbellrand-Kuruman transition zone contains three major rock types: carbonaceous limestone which is locally pyrite rich (with minor dolomite and chert), pyritic carbonaceous shale, and banded iron-formation (Fig. 2). The transition from carbonate to iron-formation occurs within a sequence that, from the base upward, grades from limestone to shale to iron-formation (Fig. 2). Contacts between limestone and shale are commonly gradational whereas those between iron-formation and shale are sharp. The iron-formations, which are light gray and lack any mesoscopically visible carbonaceous matter, contrast sharply with the carbonaceous limestone and shale units.

b

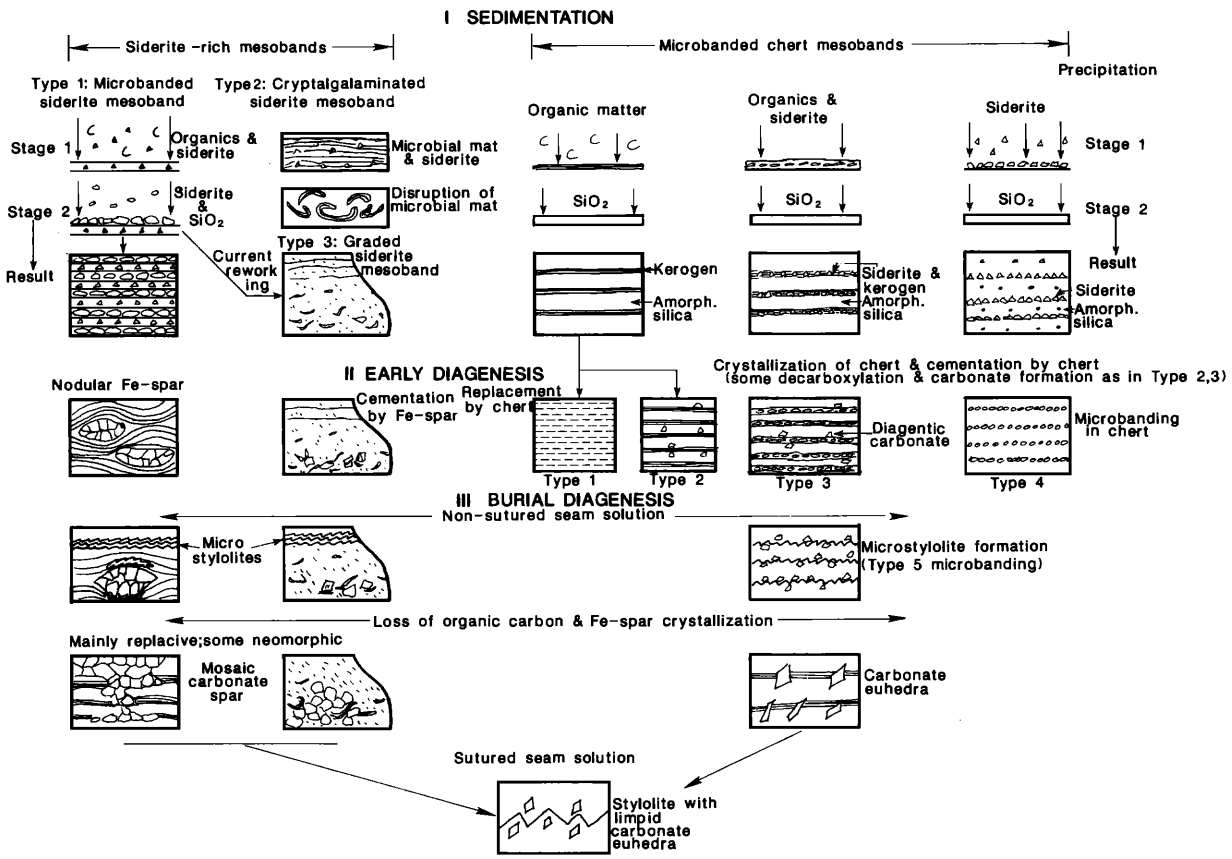

FIG. 3. (*Cont.*)

Some of the limestone units are replaced by dolomite along strike (Fig. 2; see also Beukes, 1987). The limestones comprise two major sedimentary lithofacies, with one displaying contorted microbialaminations cemented by white calcspar and the other consisting of interbedded intramicrosparite and micrite. The latter commonly grades into shale, giving rise to a subfacies of interbedded limestone-shale which is distinct from the black carbonaceous shale lithofacies (Fig. 2). Graded beds with sharp bottom contacts are common in the intramicrosparite-micrite facies.

Siderite-rich banded iron-formation is the dominant iron-formation type in the transition zone. Siderite microbanded cherts are preferentially developed along iron-formation and shale contacts (Fig. 2). Upward in the sequence, a transition to magnetite-siderite banded iron-formation marks the contact between the Kliphuis and Groenwater Members of the Kuruman Iron Formation (Fig. 2). Hematite-magnetite iron-formation is interbedded with siderite banded iron-formation in the Derby drill core (Fig. 2). Microbanding is characteristic of the banded iron-formation; however, some siderite mesobands are intraclastic or contain contorted microbialaminae (Fig. 2; see also Klein and Beukes, 1989).

All rock types in the transition zone have been sampled in each of the three cores. Further, some samples have also been collected higher in the sequence in core AD-5 at Pomfret (Fig. 2). Of these, samples 92.5, 94.4, and 121.3 contain abundant minnesotaite. The development of minnesotaite is related to the metamorphic effects of a mafic sill intruded immediately above sample 92.5. One of the samples close to the sill (AD-5-93.1) contains contorted microbialaminae composed of magnetite set in ferruginous dolomite spar (Fig. 2) (Klein and Beukes, 1989).

Carbonate and Kerogen Petrography

Major petrographic features of the various lithofacies are schematically summarized in Figure 3. The paragenetic pathways are broadly similar in all lithofacies with carbonate and kerogen occurring in four major relationships: (1) kerogen as pigmentation in

microsparite, (2) kerogen and carbonate particles as reworked detritus, (3) kerogen pigment segregated from carbonate spar, and (4) kerogen displaced by carbonate.

In all lithofacies, the earliest form of carbonate preserved appears to be microsparite pigmented by light brown kerogen. This is most conspicuous in the contorted microbialaminated limestones, in which kerogen pigmentation clearly defines primary benthic microbial mat textures (Fig. 4a). Such textures are also preserved in some siderite microsparite mesobands (Fig. 4b) in siderite-rich banded iron-formation (Fig. 3b). However, kerogen-stained siderite microsparite microbands (without microbialamination), alternating with kerogen-free to kerogen-poor siderite or chert microbands, are most common in the siderite-rich iron-formations (Fig. 3b). Neomorphic recrystallization of microsparite to sparite commonly retains some of the kerogen pigmentation.

In both limestone and siderite-rich iron-formation, some of the kerogen-pigmented microsparite has been reworked by current action (most probably density currents; Beukes, 1984) to yield graded intraclastic limestone or siderite beds, respectively (Fig. 3a and b). Clasts are commonly composed of kerogen-pigmented microsparite which either floats in a matrix of fine-grained clastic-textured carbonate mud or is cemented by coarse sparite (Klein and Beukes, 1989). In the finer grained muddy tops of graded beds, preferential sorting of carbonate mud and organic materials resulted in alternating kerogen-rich and kerogen-poor laminae, with kerogen forming the matrix for carbonate particles. The kerogen is commonly concentrated along bedding planes in the form of discontinuous microlenticles.

Similar sorting of organic matter has taken place in the carbonaceous shale units, but here kerogen-rich laminae alternate with siliciclastic quartz and/or chlorite-rich laminae. Small clots of black kerogen are commonly present in the shales. Under high magnification and combined with electron microprobe analysis, these were found to consist of phosphatic carbonate particles highly pigmented by kerogen (Van Wyk, 1987).

Carbonate grains with a very thin kerogen outline are characteristic of the dolomitized limestones; such rims appear to be the result of the segregation of kerogen pigmentation from carbonate grains during recrystallization. In these, very dark gray to black kerogen outlines subhedral to euhedral dolomite microsparite grains, and depositional textures have been obliterated (Fig. 4a). Such kerogen-rimmed grains may also result from the segregation of kerogen pigmentation from carbonates as a result of burial diagenetic processes such as nonsutured (microstylolitic) and sutured (stylolitic) seam solution (Fig. 3). In both processes, black kerogen becomes concentrated along solution surfaces as kerogen-free carbonates precipitate adjacent. Reprecipitated carbonate associated with microstylolites is commonly microsparitic, whereas that associated with stylolites usually consists of limpid, euhedral sparite grains. Reprecipitated grains in limestones are dolomite, and in iron-formation they are ferroan dolomite or ankerite. In the iron-formations, microstylolitic alteration of kerogenous microbands (Klein and Beukes, 1989) is common and leads to the formation of microstylolitic microbands in chert mesobands with siderite microsparite concentrated alongside (Figs. 3b and 4c). In kerogenous siderite mesobands this commonly leads to the formation of euhedral siderite microsparite in a matrix of kerogen (Fig. 4d). The formation of the microsparite clearly postdates deposition of the kerogen and predates microstylolite formation.

Textural relationships in the iron-formations and shales show that kerogen has been displaced by later coarse-grained carbonate spar. Specifically, sparite cuts across kerogenous microbands (Fig. 4c); there is no evidence of segregation of kerogen pigment around sparite euhedra, and kerogen is generally absent in the immediate vicinity. In the iron-formations, two stages of displacement are recognized. The earlier, less common, is represented by Fe carbonate spar nodules surrounded by compacted laminae (Klein and Beukes, 1989). The second stage is of late diagenetic origin cutting across compacted and cemented sedimentary laminations. It is typically represented by dolomite euhedra in carbonaceous shales, by equigranular mosaics of ferroan dolomite or ankerite in siderite-rich mesobands (Fig. 4e), and by ferroan dolomite or ankerite euhedra in chert-rich mesobands of iron-formation units (Fig. 4f). The latter carbonates are common in magnetite- and hematite-rich banded iron-formation units and are the only carbonates preserved in the metamorphosed minnesotaite-rich iron-formation units (Fig. 2) where all preexisting siderite has reacted to form minnesotaite in the presence of quartz. Optical zonation is very common in ferroan dolomite and/or ankerite rhombohedra (Fig. 4f). Rhombohedra commonly show a core of sparite with vermiform chert inclusions and a rim of limpid sparite. The sparites almost invariably contain poikilotopic inclusions of siderite microsparite (Fig. 4f). The rhombohedra are not exclusively ferroan dolomite and/or ankerite. Van Wyk (1987) also describes minor zoned siderite rhombohedra.

Kerogen and carbonate mineral grains are consistently associated but kerogen commonly occurs without associated carbonates in kerogen microbands in iron-poor chert units and as fine disseminated pigmentation in amoeboid-textured chert between iron mineral microbands. Recrystallization of amoeboid chert to mosaic chert (terminology after Fisher et al., 1967) leads to segregation of the light brown kerogen

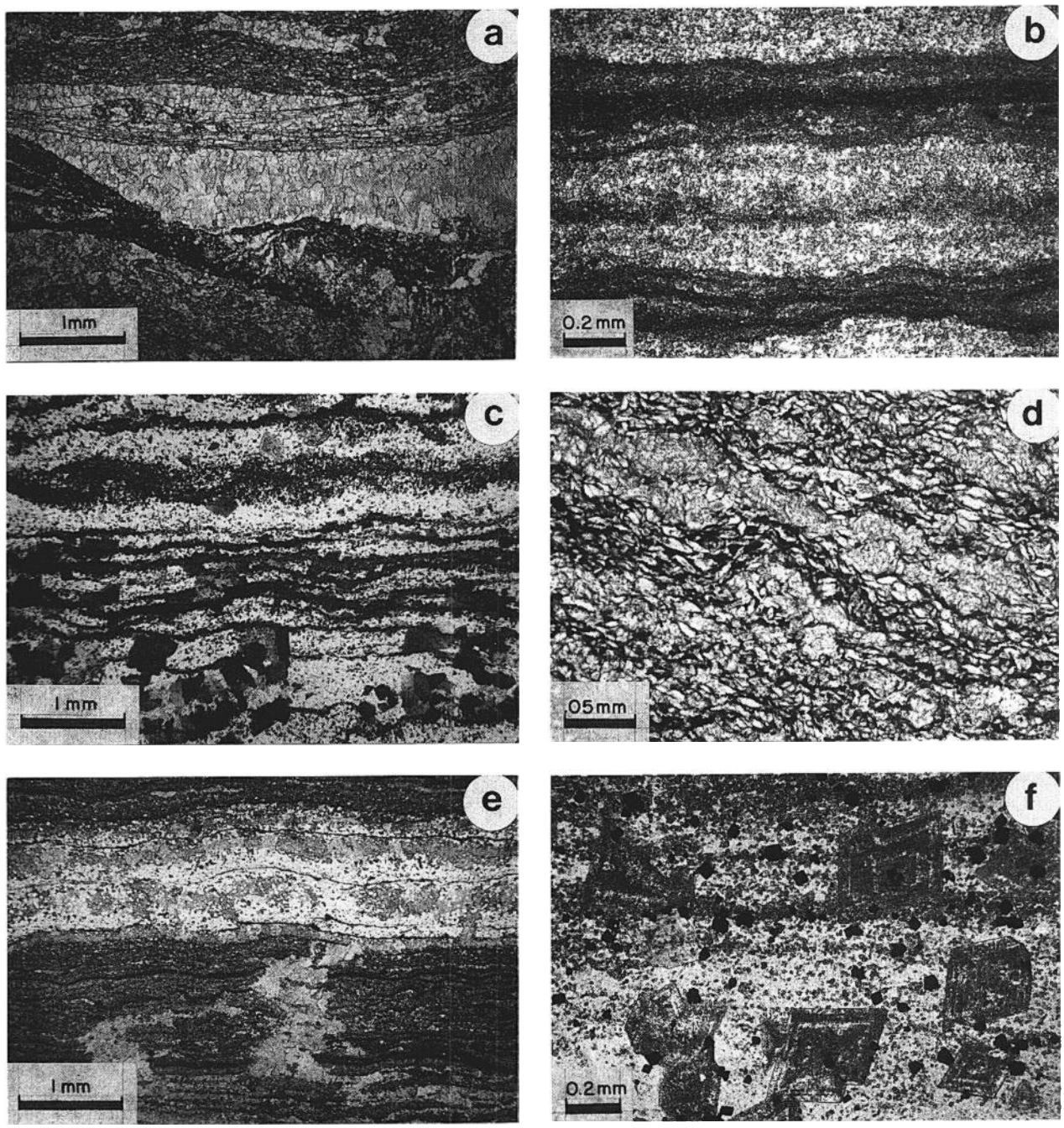

FIG. 4. Photomicrographs of various lithofacies and textures. a. Limestone showing microbialaminae and coarse spar fill in fenestrae. Grains in very dark kerogen-rich laminae are dolomite. Plane-polarized light. Sample WB-98-980.3. b. Siderite-rich iron-formation with microbands of siderite microbialaminae stained by kerogen. Plane-polarized light. Sample AD-5-163.1. c. Siderite-rich iron-formations showing many microstylolitic microbands and one microband made up of finely dispersed microsparite (one quarter down from the top of the photograph). The variably light gray to dark euhedral grains are late, cross-cutting ankerite. Partial double polarization. Sample DI-1-213.8. d. Siderite-rich iron-formation consisting of euhedral siderite grains in a dark kerogenous matrix. Plane-polarized light. Sample WB-98-800. e. Patches (light gray) of ferroan dolomite (to ankerite in composition) cutting across well-laminated siderite-rich mesobands. Plane-polarized light. Sample DI-1-223.8. f. Coarse-grained, euhedral, zoned ankerites, with poikilotopic inclusions of siderite cutting across siderite microbands in chert. Plane-polarized light. Sample AD-5-152.1.

pigment from the chert and subsequent formation of very fine, dark kerogen rims about hexagonal microquartz grains.

Carbonates not associated with kerogen are represented by sparry cements in the intraclastic carbonates, by sparry fenestral infills in contorted microbialaminated limestone (Fig. 4a), by siderite-magnetite units, and by some siderite microsparite microbands (Fig. 4f) in banded iron-formation. Cements and void-filling spars in the intraclastic and contorted microbialaminated limestones are made of calcite whereas those in siderite-rich iron-formation normally consist of ferroan dolomite or ankerite.

Relationships between iron oxide minerals (hematite and magnetite), kerogen, and carbonate minerals in the iron-formations should be noted. Kerogen is normally absent in any microscopically observable quantities in magnetite- and hematite-rich iron-formations. This is especially the case in hematite-rich units. If present, the kerogen occurs as pigmentation in chert microbands between iron oxide microbands. Dusty red hematite as pigmentation in chert and concentrated along microbands appears to be one of the earliest oxide minerals preserved in the iron-formation. It outlines original chalcedonic microspheroids in chert and, upon recrystallization, forms fine-grained specularite (Beukes, 1984). In some cases specularite and Fe microsparite (siderite, ankerite, or ferroan dolomite) are finely intergrown.

Two varieties of magnetite occur; these are (1) fine-grained, anhedral to subhedral grains intergrown with chert which may alternate with siderite or hematite microbands, and (2) coarse euhedral grains cutting across siderite and hematite. Examples are known of hematite microbands in chert pods that grade laterally into magnetite microbands outside the chert pod. Similarly siderite microbands may be replaced along strike by euhedral magnetite in transition zones between siderite- and magnetite-rich iron-formation units. Almost invariably the growth of euhedral magnetite grains has obliterated most of the primary sedimentary textures and structures. Some dispersed euhedral magnetite is almost certainly of low-grade metamorphic origin as it occurs as overgrowths on earlier anhedral magnetite and as replacement of late diagnetic ankerite rhombohedra.

Geochemistry

Analytical methods

Carbon and oxygen isotope compositions of carbonates and carbon isotope compositions and abundances of total organic carbon were determined for a suite of 55 whole-rock samples. The stratigraphic positions of the samples are shown graphically in Figure 2 and the analytical results are listed in Tables 1 to 4. In a separate publication (Klein and Beukes, 1989) the results of petrographic, electron microprobe, and elemental analyses are reported on the same suite of samples. Whole-rock samples were fragmented and crushed in a Plattner mortar and pestle and ground to a fine powder in an agate mortar and pestle. Thin sections used in the petrographic examination of carbonates and kerogens were cut from rock chips adjacent to the analytical samples.

Iron-rich and iron-poor carbonate minerals were treated with H_3PO_4 ($\rho \geq 1.89$ g/ml^{-1}) at 50°C for 48 hr (Wachter and Hayes, 1985) to produce CO_2. Although quantitative yields of CO_2 from siderites and ankerites were not possible with such a short reaction time and low temperature, the isotopic composition of the evolved CO_2 is equal to that obtained by methods using higher temperatures where quantitative yields were achieved (Rosenbaum and Sheppard, 1986). Sulfur dioxide was liberated from FeS_2 by the "Kiba reagent" method (Sasaki et al., 1979). The abundance and isotopic composition of total organic carbon were determined by quantitation and mass spectrometric analysis of CO_2 produced by combustion of acid-treated samples (J. T. Gelwicks et al., in prep.). Powdered samples (250 mg) were placed in Vycor tubes (9 × 150 mm) and treated sequentially with cold and hot, concentrated HCl. Residues were washed, dried, and mixed with CuO. The tubes were evacuated, sealed, and heated to 850°C for two hours, then opened in vacuo to allow recovery, purification, and analysis of CO_2.

Fractionation factors employed for calculation of δ_o values for carbonate minerals based on analysis of CO_2 prepared at 50°C were, for calcite, 1.00925; for dolomite, 1.01038; for siderite-rich iron-formation, 1.01066; and for oxide-rich iron-formation, 1.01044. The latter values were derived from fractionation factors for siderite (1.01074) and ankerite (1.01032) and the observed abundance ratios of these minerals, vis 4:1 in siderite-rich iron-formation and 1:4 in oxide-rich iron-formation. Values of fractionation factors follow Baur et al. (1985) and are consistent with values recommended by Rosenbaum and Sheppard (1986).

Isotopic compositions are denoted as follows: δ_{ca}, carbonate carbon, per mil vs. PDB; δ_{co}, organic carbon, per mil vs. PDB; δ_o, carbonate oxygen, per mil vs. PDB; δ_s, sulfur, per mil vs. CDT. The isotopic difference between carbonate and organic carbon is expressed as ϵ, per mil, where

$$\epsilon = [(\delta_{ca} + 1{,}000)/(\delta_{co} + 1{,}000) - 1] \times 10^3.$$

Ranges in kerogen contents and isotopic composition

Results are summarized in Table 1 for limestones and dolomites, Table 2 for shales, Table 3 for siderite-rich iron-formations and chert, and Table 4 for oxide-rich iron-formations. Also included in the tables are

TABLE 1. Partial Chemical Analyses and Isotopic Compositions of Fe-rich Micrite, Limestone, and Dolomite

	Fe-rich micrite		Limestone										Dolomite			
Analysis no.	1	2	3	4	5	6	7	8	9	10	11	12	13	14	15	16
Borehole	AD5	AD5	AD5	WB98	WB98	AD5	AD5	AD5	WB98	DI1	DI1	WB98	AD5	AD5	AD5	AD5
Depth (m)	93.10	163.40	176.90	981.00	940.00	179.80	181.70	193.40	980.30	229.30	230.20	915.00	175.20	217.20	203.60	219.00
Facies[1]	MM-D	MS	MC-S	MC-S-P-A	MC	MC-A	MC-A	MC-A	MC-A	MC-I	MC-I	MC-I	MD	MD	MD-A	MD-A
Wt %																
$C_{organic}$	0.041	0.36	1.701	2.2	1.168	2.792	0.518	0.893	0.593	0.188	0.126	0.811	0.894	0.303	0.411	0.485
Al_2O_3	0.36	0.68	8.13	4.69	1.50	4.87	1.70	0.98	0.90	1.70	0.90	3.90	2.32	1.00	2.50	1.10
FeO[2]	33.56	32.22	5.07	31.38	1.17	4.16	2.92	3.16	2.40	3.33	3.08	1.84	3.93	2.29	3.17	3.14
P_2O_5	0.030	0.128	0.138	0.055	0.069	0.072	0.028	0.190	0.089	0.080	0.070	0.080	0.094	0.051	0.040	0.040
S	0.020	0.990	3.490	17.730	0.055	0.812	0.400	1.410	0.410	1.220	0.044	0.220	0.145	0.631	0.438	0.410
Ppm																
Ba	<20	13	172	66	42	76	19	17	26	10	50	47	41	8	26	12
Th	0.371	0.629	7.660	5.170	1.690	4.200	1.310	0.364	0.727	1.840	[3]	4.320	2.240	0.587	1.470	0.952
Ppt[4]																
δ_{co}	−36.0	−35.6	−40.9	−40.7	−41.4	−36.2	−38.8	−36.5	−41.1	−36.5	−34.3	−34.9	−33.9	−32.7	−33.9	−35.6
δ_{ca}	−7.4	−1.9	−2.4	−2.0	−1.3	−2.8	−2.1	−0.5	−1.0	−0.6	−0.9	−1.3	−2.3	−0.3	−0.5	−0.1
ϵ[5]	29.7	34.9	40.1	40.3	41.8	34.7	38.2	37.4	41.8	37.3	34.6	34.8	32.7	33.5	34.6	36.8
δ_o	−13.1	−7.0	−10.3	−7.9	−9.7	−9.6	−10.3	−9.9	−8.6	−10.5	−10.4	−9.2	−9.3	−4.7	−5.9	−3.9
δ_s		−3.8				−3.5	−5.9	6.3								13.8

[1] Facies code: A = microbialaminated; I = intraclastic; MC = micrite, calcareous; MD = micrite, dolomitic; MC-S = micrite, calcareous, shaly; MM = micrite with magnetite; MS = micrite, sideritic; P = pyrite rich

[2] Total Fe as FeO

[3] Open space means value not determined

[4] Ppt = parts per thousand

[5] $\epsilon = [(\delta_{ca} + 1{,}000)/(\delta_{co} + 1{,}000) - 1]1{,}000$

TABLE 2. Partial Chemical Analyses and Isotopic Compositions of Shales

Analysis no.	1	2	3	4	5	6	7	8	9	10
Borehole	AD5	AD5	AD5	AD5	AD5	AD5	AD5	WB98	WB98	WB98
Depth (m)	157.70	163.70	176.10	181.50	169.00	188.20	188.30	826.00	853.00	926.00
Facies[1]	FS-C	FS-C	SC-P	SC-P	SC	SC	SC	SC	SC	SC
Wt %										
$C_{organic}$	5.328	3.767	2.620	2.727	4.952	6.365	3.841	4.187	2.794	2.515
Al_2O_3	15.40	7.36	5.44	8.89	12.93	11.41	8.37	12.28	6.68	6.70
FeO^2	27.56	21.68	30.23	28.40	8.35	3.04	5.97	6.46	11.01	5.44
P_2O_5	0.091	0.055	0.074	0.071	0.106	0.058	0.054	0.081	0.084	0.090
S	0.460	0.530	20.280	13.620	0.240	1.550	3.960	0.370	0.630	0.720
Ppm										
Ba	<30	9	121	98	252	174	149	263	101	142
Th	18.500	10.700	8.410	8.710	19.300	9.400	8.360	12.800	7.540	6.940
Ppt[4]										
δ_{co}	−34.6	−35.4	−38.4	−39.4	−35.3	−36.7	−36.5	−37.8	−36.4	−35.2
δ_{ca}	[3]	−4.3	−5.4	−2.4	−3.4		−2.0	−4.2	−3.6	−3.0
ϵ[5]		32.24	34.32	38.52	33.07		35.81	34.92	34.04	33.37
δ_o		−9.5	−11.6	−11.5	−11.1		−12.0	−11.4	−12.7	−9.4
δ_s			21.0		1.0	−0.3				

[1] Facies code: C = carbonaceous, F = ferruginous, P = pyrite rich, S = shale
[2] Total Fe as FeO
[3] Open space means value not determined
[4] Ppt = parts per thousand
[5] $\epsilon = [(\delta_{ca} + 1{,}000)/(\delta_{co} + 1{,}000) - 1]1{,}000$

abundances of selected major and trace elements (from Klein and Beukes, 1989) which display pertinent correlations with kerogen contents. Contents of organic C range from a low of 0.01 wt percent in oxide-rich iron-formations (Table 4) to a high of 6.36 wt percent in shales (Table 2). Included with the limestones and dolomites (Table 1) are two femicrite-rich samples. The kerogen contents of the shales are consistently high, independent of whether their iron content is due to the presence of abundant Fe chlorite or abundant pyrite (Table 2). The kerogen contents of the siderite-rich iron-formations and chert are about tenfold lower (Table 3). One siderite-rich sample with an organic carbon content of 0.67 wt percent is known to contain shale partings (Table 3, analysis 17). Oxide-rich iron-formations have very low kerogen contents ranging between 0.02 and 0.01 wt percent organic carbon (Table 4).

The kerogens are highly depleted in ^{13}C, with δ_{co} ranging from a low of −41.4 per mil in limestone (Table 1) to a high of −24.6 per mil in oxide-rich iron-formation. The range of δ_{co} values in the shales is −34.6 to −39.4 per mil (Table 2), approximately similar to that of the limestones (Table 1), while that of the siderite-rich banded iron-formations and chert is from −27.2 to −38.5 per mil (Table 3). Kerogens in the oxide-rich iron-formations are less depleted in ^{13}C, with a δ_{co} range of −24.6 to −28.9 per mil (Table 4).

The carbonates in the limestones and dolomites are only slightly depleted in ^{13}C, with δ_{ca} values ranging from −0.1 to −2.8 per mil (Table 1). In contrast, the carbonates in the oxide-rich iron-formation are very markedly depleted with values ranging between −5.0 and −13.7 per mil (Table 4). Carbonates in the shales are slightly more depleted in ^{13}C than those from limestone and dolomite, with a range of −2.0 to −5.4 per mil (Table 2). Intermediate between shales and oxide-rich iron-formations are the siderite-rich iron-formations with δ_{co} values ranging from −3.0 to −7.9 per mil (Table 3).

The carbon isotope difference between carbonates and kerogen is largest in the limestones and dolomites, with ϵ values ranging between 29.7 and 41.8 per mil (Table 1). Isotopic differences are much lower in the oxide-rich iron-formations, ranging from 12.8 to 22.4 per mil (Table 4).

Oxygen isotope compositions range from −3.9 in dolomite (Table 1) to −14.4 in minnesotaite-rich iron-formation (Table 4). The range of ^{18}O contents is, however, narrowed considerably if the effects of ^{18}O enrichment in dolomite (Table 1) and ^{18}O depletion in minnesotaite- and hematite-rich iron-formations (Table 4), relative to other rock types, are taken into consideration.

Isotopic compositions of pyritic sulfur in samples from drill core AD-5 have a very wide range from −5.9 to 21.0 per mil vs. Canyon Diablo troilite (CDT) and do not appear to be lithofacies controlled (Tables 1, 2, and 3). Details of the pyrite petrography are given in Klein and Beukes (1989).

Average compositions and standard deviations of populations for the various lithofacies are given in

Table 5. Differences in the average carbon isotope compositions of the various lithofacies (Table 5) are illustrated in Figure 5. Some interesting crossovers occur. Kerogens in the limestones and shales are on average most depleted in ^{13}C, with δ_{co} values around −37 per mil. Siderite-rich iron-formations and dolomites grouped together are somewhat less depleted in ^{13}C, with δ_{co} values between −33 to −34 per mil (Fig. 5). However, the carbonates in the limestones and dolomites are grouped together as the least depleted in ^{13}C (at about −1‰), with the shales more depleted (at −3.5‰), and the siderite-rich iron-formations even more so (at −5.3‰). On average, the oxide-rich iron-formations are least depleted in ^{13}C in kerogen ($\delta_{co} = -26.1$) and most depleted in carbonate minerals ($\delta_{ca} = -9.2$) (Fig. 5). The average δ_o values of the limestones, shales, and siderite-rich iron-formations are closely grouped around −10 per mil, with the dolomites markedly enriched in ^{18}O at −5.9 per mil and the oxide-rich iron-formations most depleted at −12.0 per mil, on average (Fig. 5, Table 5).

Stratigraphic variations

Chemostratigraphic plots (Fig. 6a, b, and c) show that kerogen is concentrated in the shales and depleted in the iron-formations with intermediate values in the limestone and dolomites. Depletion of ^{13}C in the carbonates increases upward in stratigraphic transitions from limestone and shale into iron-formation. This depletion is coupled with an enrichment of ^{13}C in the kerogen component of the rocks. This is especially well illustrated in borehole cores AD-5 and WB-98 (Fig. 6a and b). The same effect is seen in borehole DI-1 although less dramatically so because of a smaller variation in rock types. Most conspicuous in the latter is the ^{13}C enrichment in kerogen associated with hematite-containing iron-formation relative to that in the siderite-rich iron-formations and limestones (Fig. 6c). Notably, enrichment of ^{13}C in the kerogen from the hematite-rich samples is not coupled with depletion of ^{13}C in the carbonates.

Carbonates most depleted in ^{13}C are from the minnesotaite-rich iron-formation units close to the diabase sill in core AD-5 (Fig. 6a). These contain sparry ankerite rhombohedra and no siderite. Within the contact metamorphic aureole of the same sill, dolomite in a magnetite-rich sample with contorted microbialaminae has an isotopic composition similar to that of siderites lower in the sequence. The isotopic composition of the kerogen in this sample is also of the same order as that of siderite-rich iron-formation (Fig. 6c). One sample of pyritic shale in core AD-5 contains dolomite exceptionally depleted in ^{13}C (Fig. 6a; Table 2, analysis 3).

The oxygen isotope variations along the chemostratigraphic curves are rather gentle illustrating the similarity in ^{18}O contents of the carbonates in the limestones, shales, and iron-formations. However, marked peaks indicating enrichment in ^{18}O are associated with dolomite and siderite micrite in core AD-5 (Fig. 6a). In contrast, samples of magnetite- and minnesotaite-bearing iron-formations from the metamorphic aureole of the sill in AD-5 are markedly depleted in ^{18}O (Fig. 6a). The two hematite-rich iron-formation samples in borehole core DI-1 (Fig. 6c) are also depleted in ^{18}O relative to other core samples.

Element correlations

Total organic carbon (kerogen) contents correlate positively with ^{13}C enrichment in carbonates (Fig. 7a) and negatively with ^{13}C in organic matter (Fig. 7b). The result is a strong positive correlation between ϵ values and total organic carbon contents, with oxide-rich iron-formations displaying the lowest values (Fig. 7c). In contrast, organic carbon contents and δ_o values appear unrelated with the exception that some dolomites relatively rich in organic carbon are enriched in ^{18}O, and minnesotaite- and hematite-rich iron-formations containing virtually no organic carbon are depleted in ^{18}O relative to other lithofacies (Fig. 7d).

Depletion of ^{13}C in carbonates is correlated with total iron content (expressed as FeO, Fig. 8a). Cross plots of δ_{co} and ϵ against FeO reflect carbon isotope correlations noted above, but show more complex structure (Fig. 8b and c). Total organic carbon abundance is negatively correlated with abundance of FeO (Fig. 9). Relatively heavy O ($\delta_o > -6$ vs. PDB) is found only in samples with lower iron contents (Fig. 8d).

Correlations between the various parameters are possible only for the overall groupings of lithofacies. Within a grouping of a specific lithofacies, parameters often appear to vary independently of each other, such as for example in the cross plots of organic carbon and various isotopic ratios (Fig. 7). Let us look in somewhat more detail at the overall groupings of lithofacies in the various cross plots. Figure 7a shows independent trends for iron-formation on the one hand and the dolomite-limestone-shale grouping on the other. In the iron-formation assemblage, organic carbon correlates positively with ^{13}C enrichment but in the dolomite-limestone-shale assemblage it correlates negatively. The same applies to ϵ (Fig. 7c) and δ_o (Fig. 7d) plotted against carbon. This relationship is again illustrated in the cross plot of total organic carbon and iron contents (Fig. 9). In the grouping of limestone-dolomite-shale there is a positive correlation between carbon and iron contents but in the distribution of iron-formation data points there is a strong negative correlation (Fig. 9). In the cross plots of organic carbon versus isotopic ratios (Fig. 7) and total iron contents (Fig. 9) iron-formations are clearly separated from the shales by limestone, yet in a stratigraphic sense shale normally separates iron-formation from limestone (Fig. 2). It is only in the cross plots of

TABLE 3. Partial Chemical Analyses and Isotopic

Analysis no.	1	2	3	4	5	6	7	8	9
Borehole	AD5	AD5	AD5	AD5	AD5	AD5	AD5	AD5	DI1
Depth (m)	121.30	158.40	159.30	161.90	161.95	163.20	167.80	168.70	213.80
Facies[1]	BS	BS	B	BS	BS	BS	BS	BS	BS
Wt %									
$C_{organic}$	0.052	0.047	0.110	0.060	0.060	0.144	0.065	0.101	0.041
Al_2O_3	0.02	0.05	0.09	0.13	0.10	0.29	0.15	0.14	0.04
FeO[2]	27.46	27.12	22.14	34.40	24.88	17.18	24.96	27.19	22.72
P_2O_5	0.064	0.052	0.029	0.101	0.078	0.029	0.110	0.102	0.084
S	0.049	0.019	0.013	0.037	0.230	0.032	0.019	0.150	0.060
Ppm									
Ba	<15	<15	<20	<20	<20	<20	<20	13	<30
Th	<0.035	<0.04	0.033	0.114	0.028	0.377	0.142	0.078	[3]
Ppt[4]									
δ_{co}	−30.8	−30.1	−32.8	−29.7	−27.2	−34.9	−32.2	−32.3	−31.3
δ_{ca}	−6.9	−5.3	−4.4	−3.8	−3.0	−3.0	−4.9	−4.5	−5.9
ϵ[5]	24.66	25.57	29.36	26.69	24.88	33.05	28.21	28.73	26.22
δ_o	−10.7	−9.5	−10.2	−9.7	−8.4	−10.3	−11.0	−10.9	−11.5
δ_s				3.9				−2.8	

[1] Facies code: B = banded iron-formation (BIF), BS-S = siderite BIF with shale, CC = carbonaceous chert, CS = sideritic chert, S = siderite

[2] Total Fe as FeO

[3] Open space means value not determined

[4] Ppt = parts per thousand

[5] $\epsilon = [(\delta_{ca} + 1{,}000)/(\delta_{co} + 1{,}000) - 1]1{,}000$

total iron versus isotopic ratios (Fig. 8) that a link exists between shale and iron-formation due to enhanced pyrite contents or the presence of Fe-rich chlorites in the shales.

Oxygen isotope ratios appear to vary independently of carbon isotope ratios for specific lithofacies (Fig. 10). Siderite- and magnetite-rich iron-formations have similar oxygen isotope ratios but differ in their carbon isotope ratios (Fig. 10). These diagrams illustrate the depletion of ^{18}O in metamorphic iron-formation samples close to the diabase sill and in the two hematite-rich iron-formation samples. In contrast, dolomite samples and one siderite micrite sample are distinctly enriched in ^{18}O. Taking all lithofacies into consideration, there is a positive correlation between ^{18}O and ^{13}C in the carbonate minerals (Fig. 10a) but no correlation between δ_o and δ_{co} (Fig. 10b). The weak positive correlation between ϵ and δ_o (Fig. 10c) is thus related to variations of ^{13}C values in the carbonate minerals. The limestone-dolomite-shale assemblage displays the highest carbon isotope fractionation between carbonate minerals and organic matter and the oxide-rich iron-formations show the least; the siderite-rich iron-formations show intermediate values (Fig. 10c).

Discussion

On account of the complex paragenetic history of the carbonate minerals and kerogen in the various lithofacies (Fig. 3) it is important to try to evaluate the possible effects of any postdepositional alterations on the whole-rock analytical results. In this study such an assessment is possible because of a detailed knowledge of the petrography and geologic setting of the samples.

Metamorphic and deep burial diagenetic effects

Late diagenetic sparry ankerites are isotopically more depleted in ^{13}C than siderites as concluded from the isotopic composition of the siderite-poor, ankerite-rich oxide iron-formations versus siderite-rich iron-formations. Sparry ankerites and/or ferroan dolomites are abundant carbonates in these oxide-rich iron-formations (Klein and Beukes, 1989) and on average the oxide-rich iron-formations are depleted in ^{13}C relative to siderite-rich iron-formations by 3.9 per mil (Table 5, Fig. 5). The euhedral shape and generally limpid nature of these sparry carbonate grains would suggest that under the given low-temperature diagenetic conditions, they formed by very slow crystallization from highly dilute formation water (Folk, 1974); the composition of such water must have varied with time to produce optically visible zoning (Van Wyk, 1987). The water must also have been depleted in soluble iron and enriched in Ca and Mg relative to that from which the earlier siderites precipitated. The euhedral grains appear to have formed after complete lithification of the sediment through replacement of quartz and poikilotopic incorporation of siderite microsparite (Fig. 4f). Kerogen also appears to have been displaced by the euhedra and it is therefore probable that they formed during a period of deep

Compositions of Siderite-rich Iron-Formation and Chert

10	11	12	13	14	15	16	17	18	19
DI1	DI1	DI1	WB98	WB98	WB98	WB98	DI1	WB98	DI1
223.80	236.70	237.00	814.30	816.90	886.00	882.00	221.50	896.10	245.20
BS	BS	BS	BS	B	BS	BS	BS-S	CS	CC
0.084	0.062	0.203	0.059	0.065	0.061	0.061	0.673	0.104	0.146
0.12	0.05	0.11	0.05	0.13	0.06	0.06	1.30	0.21	0.28
19.24	21.31	38.98	26.87	21.26	26.38	15.78	26.15	13.21	7.98
0.007	0.055	0.028	0.030	0.046	0.095	0.080	0.084	0.012	0.013
0.012	0.024	0.032	0.023	0.033	0.016	0.019	0.260	0.100	0.048
<30	<10	<30	<10	9	<20	<30	7	7	<15
	0.048	0.123	<0.04	<0.05	0.057	0.024	2.160	0.174	0.267
−35.6	−38.5	−37.2	−35.7	−34.9	−32.6	−34.4	−37.3	−35.6	−37.9
−4.7	−7.9	−6.7	−6.9	−6.6	−4.2	−5.7	−3.7	−4.4	−4.5
32.04	31.83	31.68	29.87	29.32	29.36	29.72	34.90	32.35	34.72
−11.9	−11.2	−10.3	−10.6	−10.6	−10.3	−10.2	−11.5	−10.0	−9.4

burial thermal degradation with the light carbon isotope signature derived from organic carbon (Coleman, 1985). A similar process must have been responsible for the formation of the postcompactional dolomite rhombohedra in the carbonaceous shales; these are depleted in ^{13}C by on average 2.2 per mil relative to associated limestone and dolomite (Table 5).

The conclusion is, therefore, that the relatively light isotopic signature of the oxide-rich formations is a function of the abundance of sparry carbonates

TABLE 4. Partial Chemical Analyses and Isotopic Compositions of Oxide-rich Iron-Formations

Analysis no.	1	2	3	4	5	6	7	8	9	10
Borehole	AD5	AD5	AD5	DI1	DI1	AD5	AD5	AD5	WB98	WB98
Depth	92.50	94.40	124.80	226.10	238.80	136.50	149.80	152.10	791.20	791.40
Facies[1]	BMi	BMi	BMi	BH	BH	BH	BM	BM	BM	BM
Wt %										
$C_{organic}$	0.010	0.017	0.008	0.015	0.013	0.015	0.008	0.008	0.013	0.015
Al_2O_3	0.07	0.18	0.04	0.11	0.08	0.04	0.04	0.03	0.04	0.03
FeO[2]	33.31	48.64	43.17	31.27	30.64	41.80	34.90	33.16	43.07	40.18
P_2O_5	0.083	0.101	0.088	0.122	0.343	0.115	0.060	0.061	0.085	0.041
S	0.049	0.018	0.004	0.010	0.007	0.011	0.007	0.006	0.004	0.003
Ppm										
Ba	<30	<15	<20	<20	<20	<25	<15	<10	<35	<25
Th	0.058	0.146	<0.05	0.074	0.036	0.029	<0.05	<0.035	<0.06	<0.04
Ppt[4]										
δ_{co}	−26.2	−26.4	−25.8	−27.5	−25.8	−25.1	−25.5	−24.6	−28.9	−25.5
δ_{ca}	−13.7	−13.6	−9.0	−5.7	−5.0	[3]	−8.2	−7.9	−9.7	−9.7
ϵ[5]	12.84	13.15	17.24	22.42	21.35		17.75	17.12	19.77	16.21
δ_o	−14.4	−13.2	−10.6	−13.1	−13.6		−11.9	−10.7	−10.3	−10.8

[1] Facies code: B = banded iron-formation (BIF), H = hematitic (in addition to magnetite), M = magnetite-rich, Mi = minnesotaite-rich (in addition to magnetite)

[2] Total Fe as FeO

[3] Open space means value not determined

[4] Ppt = parts per thousand

[5] $\epsilon = [(\delta_{ca} + 1{,}000)/(\delta_{co} + 1{,}000) - 1]1{,}000$

TABLE 5. Average Compositions of Various Lithofacies (averages based on Tables 1–4)

	Limestone			Dolomite			Shale			Siderite iron-formation			Oxide iron-formation		
	Avg	St. dev.[1]	No. analyses	Avg	St. dev.	No. analyses	Avg	St. dev.	No. analyses	Avg	St. dev.	No. analyses	Avg	St. dev.	No. analyses
Wt %															
$C_{organic}$	0.89	0.79	8	0.52	0.22	4	3.91	1.24	10	0.08	0.04	16	0.01	0.003	10
Al_2O_3	2.06	1.40	8	1.73	0.68	4	9.55	3.11	10	0.10	0.06	16	0.07	0.05	10
FeO[2]	2.76	0.87	8	3.13	0.58	4	14.81	10.31	10	24.87	5.73	16	38.01	5.83	10
P_2O_5	0.08	0.04	8	0.06	0.02	4	0.08	0.02	10	0.06	0.03	16	0.11	0.08	10
S	0.57	0.49	8	0.41	0.17	4	4.24	6.61	10	0.05	0.06	16	0.01	0.01	10
Ppm															
Ba	35.87	20.55	8	21.75	12.97	4	145.44	74.13	9	11.00	[3]	2	<20		10
Th	2.06	1.47	7	1.31	0.62	4	11.07	4.22	10	0.10	0.10	10	0.07	0.05	5
Ppt[4]															
δ_{co}	−37.47	2.53	8	−34.03	1.06	4	−36.58	1.48	10	−33.13	2.90	16	−26.12	1.17	10
δ_{ca}	−1.30	0.73	8	−0.78	0.88	4	−3.54	1.02	8	−5.29	1.41	16	−9.18	2.85	9
ϵ[5]	37.58	2.58	8	34.42	1.49	4	34.29	1.72	8	28.79	2.46	16	17.39	3.02	9
δ_o	−9.70	0.59	8	−5.90	2.05	4	−10.90	1.09	8	−10.40	0.80	16	−12.0	1.46	9
$\delta^{34}S$	Average all samples = 3.7; standard deviation = 7.89; no. of analyses = 10														

[1] St. dev. = standard deviation (σ_x)
[2] Total Fe as FeO
[3] Open space means value not determined
[4] Ppt = parts per thousand
[5] $\epsilon = [(\delta_{ca} + 1{,}000)/(\delta_{co} + 1{,}000) - 1]1{,}000$

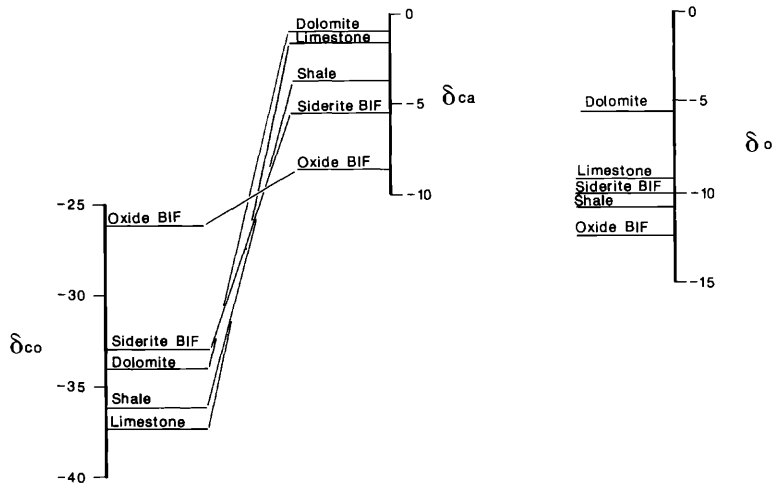

FIG. 5. Average carbon isotope (δ_{co} and δ_{ca}) and oxygen isotope (δ_o) compositions of the various lithofacies.

resulting from deep burial diagenesis (Fig. 11a). This process was apparently also a factor in the formation of postcompactional carbonate euhedra (with depleted ^{13}C values) in the shales (Fig. 11a). Late-diagenetic sparry ankerites present in siderite-rich iron-formation may have contributed significantly to ^{13}C depletion in bulk carbonate analyses from this facies, in addition to other factors to be discussed below.

The relatively low ϵ values in the oxide-rich iron-formations relative to other lithofacies (Fig. 10c) thus appear to be related to the combined effect of metamorphism and diagenetic thermal decarboxylation. Apparently the metamorphism did not alter the isotopic composition of the organic carbon significantly because the minnesotaite-rich samples have δ_{co} values similar to those of other oxide-rich iron-formations (Fig. 10b). The organic carbon in the microbialaminated magnetite-dolomite sample from the metamorphic aureole of the sill has a ^{13}C isotope composition similar to that of the siderite-rich iron-formations from which it may have been derived (Fig. 10b). The minnesotaite-rich samples illustrate that the main metamorphic reaction was one of siderite and chert forming minnesotaite, with the resulting loss of siderite from the system and lowering of the δ_{ca} values (Fig. 10a) and hence low ϵ values (Fig. 10c).

Low-grade metamorphic effects can be evaluated from the minnesotaite-rich iron-formation samples in the metamorphic aureole of the diabase sill in core AD-5. In two of these samples close to the sill no siderite remains and only sparitic euhedral ankerites depleted in ^{13}C are preserved (Fig. 6a). Carbonate in the minnesotaite-rich sample farthest from the sill (Table 4, analysis 3), which still contains some siderite, is less depleted in ^{13}C. An additional metamorphic effect has been the lowering of the ^{18}O contents of the carbonates in the minnesotaite-rich samples closest to the sill, as is also the case for the ferroan dolomite from the adjacent microbialaminated magnetite-rich sample (Table 1, analysis 1; Fig. 6a). It appears very likely that this magnetite-ferroan dolomite assemblage is the metamorphic product of an earlier siderite-ankerite assemblage because its ^{13}C values for kerogen and dolomite are similar to those of siderite-rich iron-formation (Fig. 10).

A discussion of metamorphic and thermal degradation effects must include findings of recent stable isotope studies in iron-formation from the Hamersley Range, Western Australia, which is very similar in general character and geologic setting to the Kuruman Iron Formation (Button, 1976). The positive correlation between magnetite contents and ^{13}C depletion in ankerites from the Hamersley Range (Baur et al., 1985) may be of late diagenetic and/or metamorphic origin. Becker and Clayton (1972) point out that the lightest carbonate carbon signatures in the Dales Gorge Member of the Brockman Iron Formation are associated with samples containing minnesotaite; exactly analogous to the case in borehole core AD-5 (Fig. 6a). Furthermore, carbonates (Baur et al., 1985; Kaufman et al., 1990) and chert from the Brockman Iron Formation are more depleted in ^{18}O than Kuruman Iron Formation samples (Perry and Ahmad, 1983) suggesting a somewhat higher grade of metamorphism for the Australian samples, which is supported by their mineral assemblages (Miyano and Beukes, 1984).

Effects of dolomitization

Dolomitization of the limestone was accompanied by enrichment in ^{18}O contents of 3.8 per mil on av-

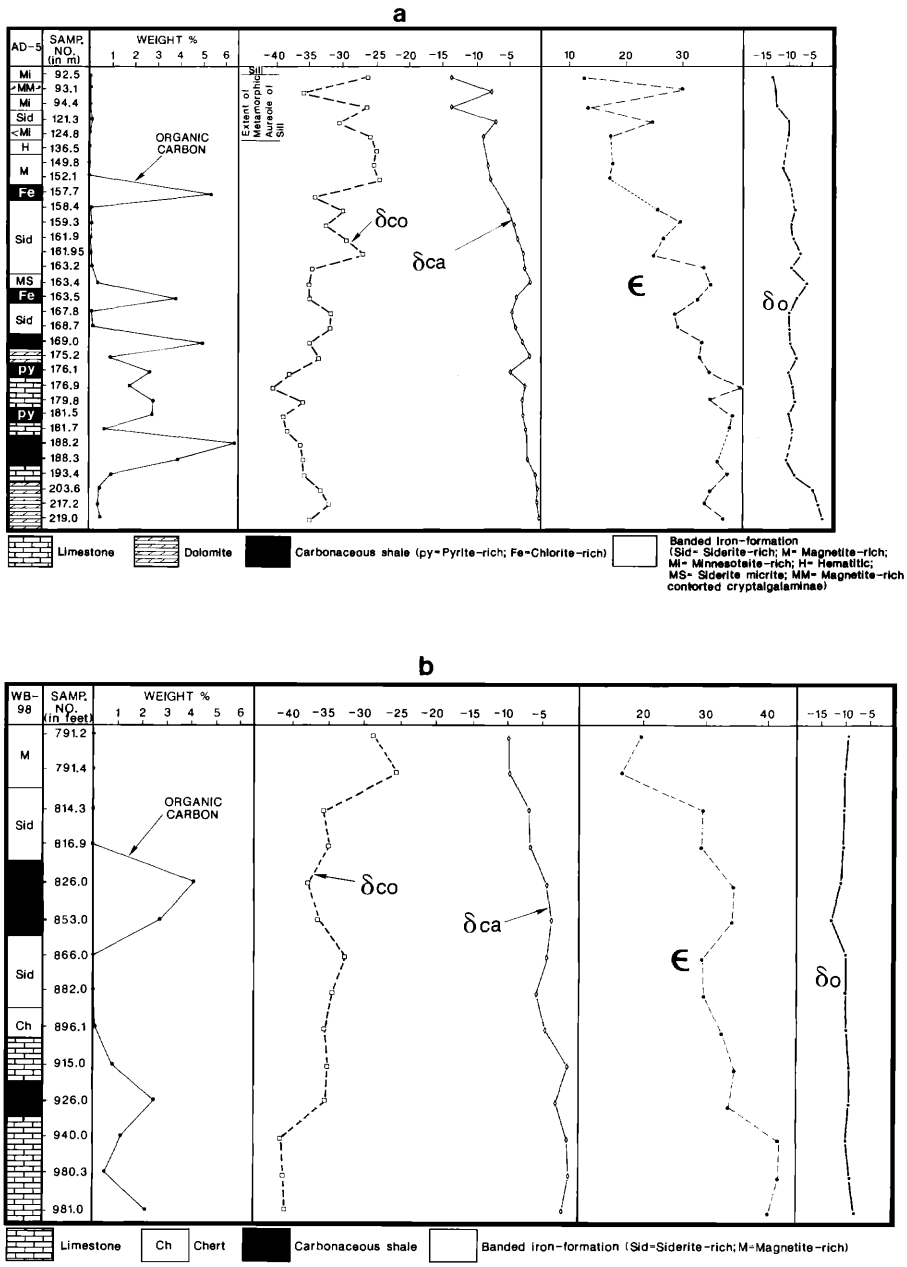

FIG. 6. Plots of total organic carbon, δ_{ca}, ϵ, and δ_o as a function of lithofacies and stratigraphic location. a. Borehole AD-5. b. Borehole WB-98. c. Borehole DI-1. Note that sample spacings are not to scale.

erage (Table 5; Figs. 5 and 10). This is somewhat lower than the 4- to 7-per mil fractionation expected experimentally between calcite and dolomite (Hoefs, 1987) but similar to the 2- to 4-per mil fractionation between natural Holocene calcite and dolomite (Land, 1980). Isotopic compositions of carbonate carbon in limestones and dolomites are similar, suggesting a lack of alteration during dolomitization (Figs. 5 and 10a). The kerogen in the dolomites appears to be slightly enriched in ^{13}C relative to that of the limestones (Figs. 5 and 10b) and this may have resulted from the loss of some isotopically light kerogen components during the recrystallization process. The fact that the color of the kerogen changes from brown in calcspar to opaque black in dolomite may reflect this greater maturation level.

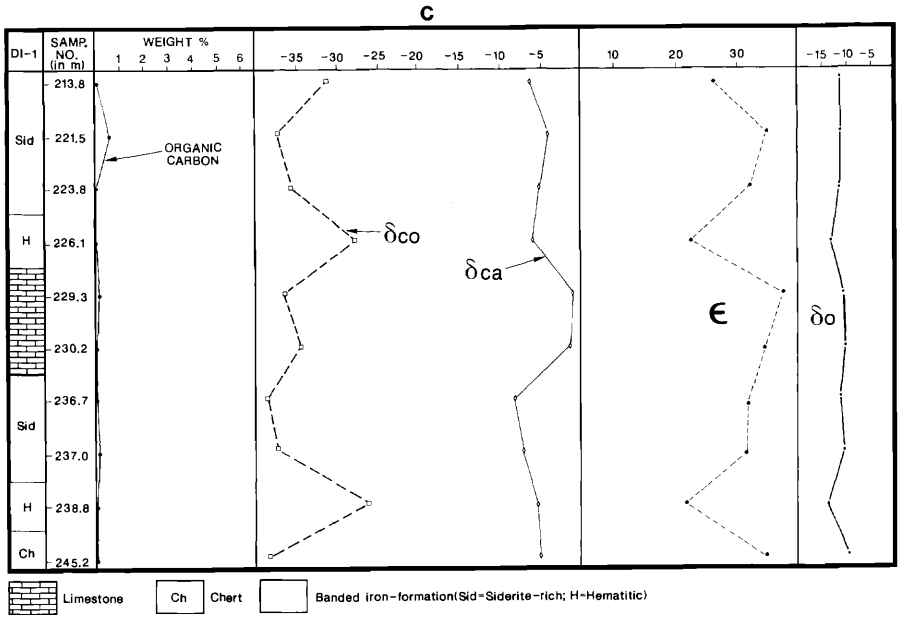

FIG. 6. (*Cont.*)

Limestone versus siderite isotope signature

The carbonate carbon isotope composition of the limestones is close to zero (Fig. 11a). The slight ^{13}C variation (−0.47 to −2.77‰) can be explained by possible incorporation of small amounts of organically derived ^{13}C-depleted carbon into the calcites; the limestones contain up to 2.79 wt percent organic carbon (Table 1). Independent of calcspar contents, the various subfacies of limestone all have approximately similar isotopic compositions. Results on microdrilled samples of sparry contorted microbialaminated limestone show that kerogenous microsparite and kerogen-free sparite have similar isotopic compositions (Table 6). This would suggest very rapid and early cementation of the contorted microbialaminae by calcspar in a system that was essentially open to surface waters of the basin. The uncompacted nature of highly contorted microbialaminae in the limestones (Fig. 4a) is strong support for this interpretation.

If the limestones reflect the total dissolved carbon isotope composition of the basin water, the question must be asked as to the significance of the isotopic signature of the interbedded siderite-rich iron-formation (which is on average depleted in ^{13}C over the limestones by 3.98‰; Table 5 and Fig. 5). This question becomes especially significant for two reasons. Firstly, it is thermodynamically predicted that siderite should be enriched by about 5 per mil in ^{13}C relative to calcite if they were precipitated from the same water mass at 25°C (Golyshev et al., 1981; Kaufman et al., in press). Secondly, some arguments can be made for much of the siderite microsparite being a primary precipitate from the basin water and not a diagenetic product as is the case for siderite in Recent marine (Berner, 1971; 1981) environments. Textural similarities between limestone and siderite units such as their microsparitic character, pigmentation by kerogen, and good preservation of primary sedimentary textures (such as microbialamination and graded bedding) make it difficult to suggest different environmental conditions for their origin. Also, there are no indications of limestone having been replaced by siderite; in fact they occur mutually exclusive of each other. Limestone is only replaced by dolomite which tends to obliterate primary sedimentary textures. Another possibility is that siderite is the diagenetic product of a ferric oxide precipitate having reacted with organic matter as a reductant (Walker, 1984). However, there is no petrographic or field evidence for large-scale replacement of iron oxides by siderite. In this respect Klein and Beukes (1989) point out that the oxide-rich iron-formations consistently contain less carbon than do the siderite-rich iron-formations suggesting that the latter could not have been derived from the former by making use of organic carbon as a reductant. Such a process is also proposed to cause ^{13}C depletion in the siderites formed (Walker, 1984), yet carbonates in the oxide-rich iron-formations are generally more depleted in ^{13}C than those in the siderite-rich iron-formations (Figs. 5 and 11a). Similarly, the isotopic composition of organic carbon in oxide-rich iron-formations is more enriched in ^{13}C than that of the siderite-rich units (Fig. 11c) and not the other way around, as would be the case if the siderite had been derived from a reaction between hematite and

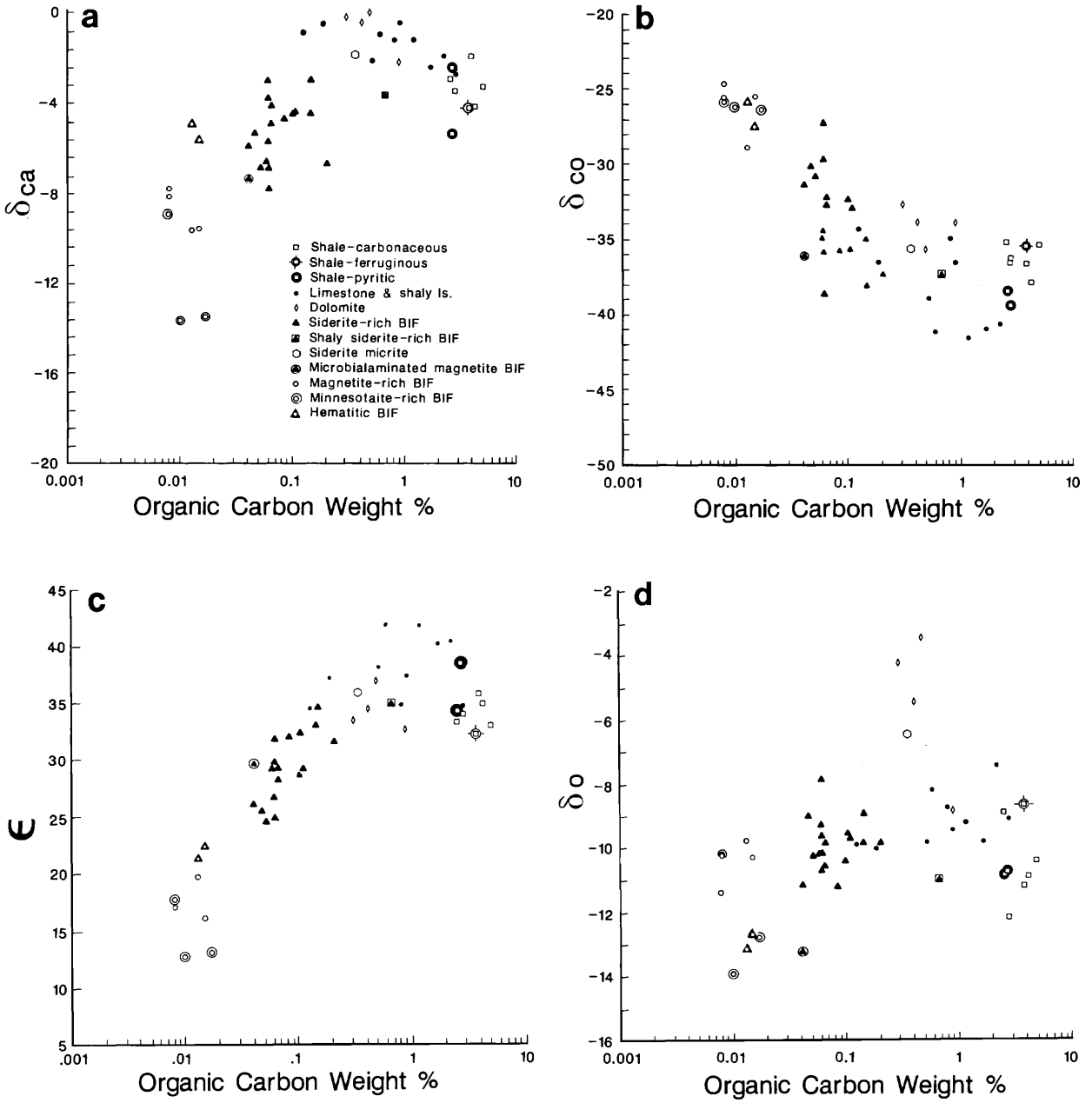

FIG. 7. Plots of organic carbon content versus isotopic measurements, identified in terms of each of the lithofacies.

organic matter. This is based on the assumption that the isotopically very light kerogen in the limestone best reflects the original isotopic composition of the organic matter.

Petrographically there is no evidence for exchange of carbon between siderite microsparites and kerogen. The isotopic compositions of the recrystallized and unrecrystallized siderites are the same. This is consistent with petrographic observations suggesting that the kerogen pigmentation merely became segregated from microsparite grains during recrystallization (Fig. 4c). Diagenetic sparitic ankerite and ferroan dolomite did, however, displace kerogen (Fig. 4e) and variations in the abundance of these minerals may account for the variance in δ_{ca} values in the siderite-rich banded iron-formation (Fig. 7a). This variance is much

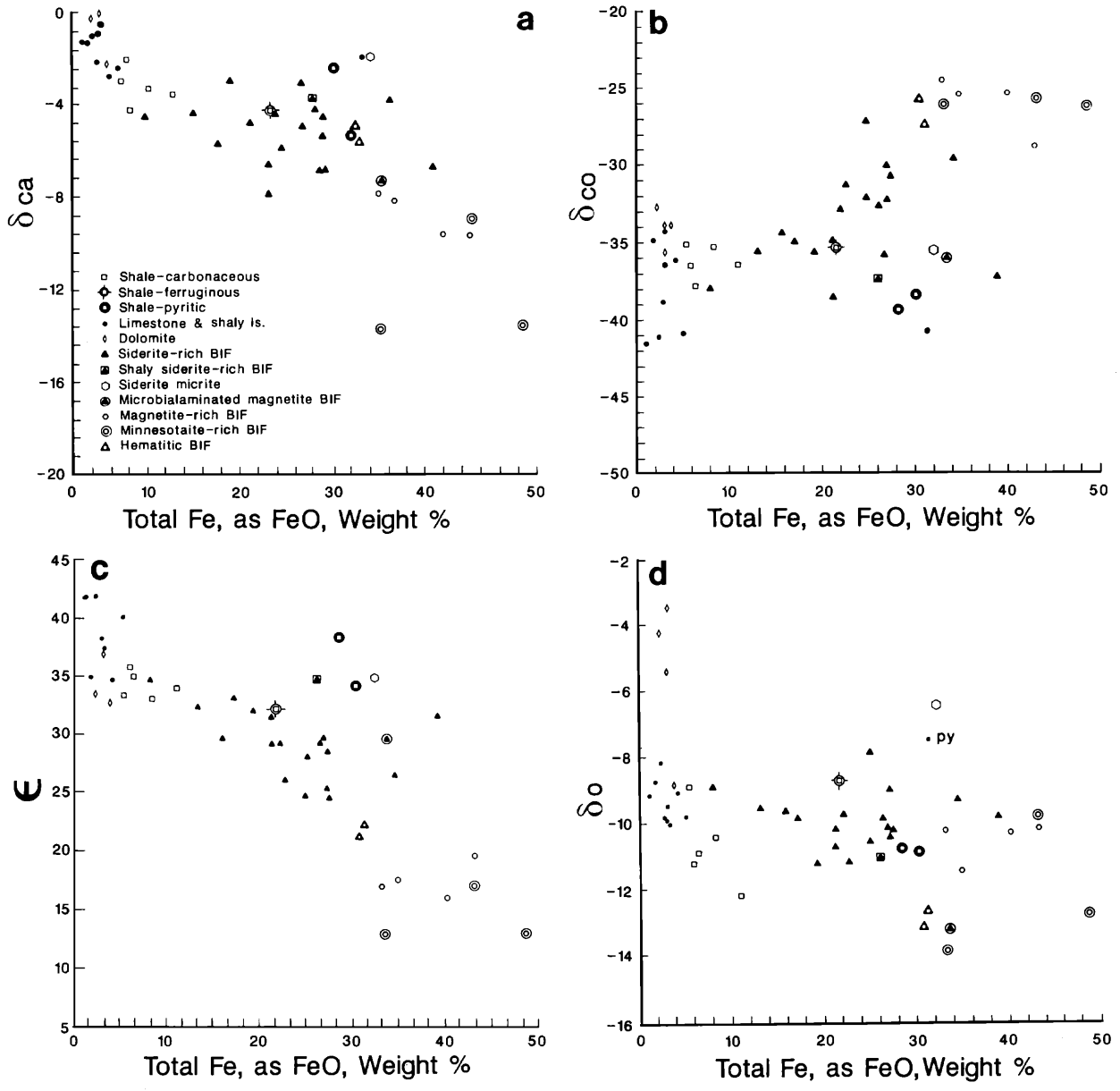

FIG. 8. Plots of total Fe content (expressed as FeO) versus isotopic measurements, identified in terms of each of the lithofacies.

larger than that in the limestone and can be attributed to the more complex diagenetic history of the carbonates in the iron-formations (Fig. 3).

Evidence for a stratified ocean system

The conclusion that both limestone and siderite are primary precipitates from a basin water, yet display different isotopic compositions, with the siderite depleted by approximately 4 per mil in ^{13}C over calcite, would imply a water column stratified with regard to isotopic composition of total dissolved CO_2. In fact, the water mass from which the siderite precipitated must have been depleted by about 9 per mil in ^{13}C over that from which calcite precipitated if thermodynamic fractionation between the two carbonate species at 25°C (Golyshev et al., 1981; Kaufman et al., in press) is taken into account. This principle of a stratified water column would fit very well with the stratified ocean model developed by Klein and Beukes (1989) for deposition of the Campbellrand-Kuruman

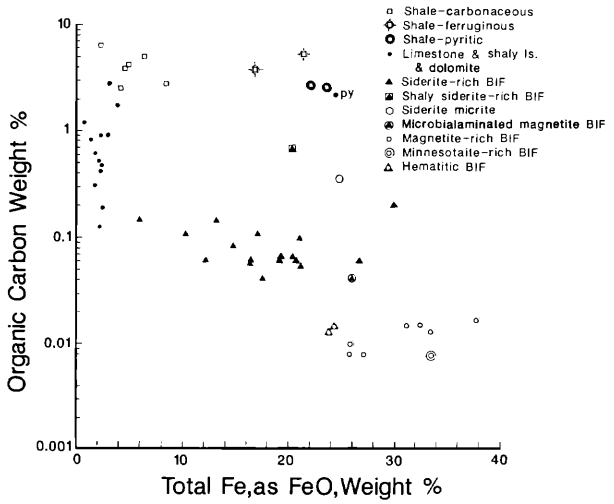

FIG. 9. Plot of organic carbon versus total Fe (expressed as FeO), identified in terms of each of the lithofacies.

transition zone. This model, based on major and trace element compositions, rare earth element patterns, and kerogen contents of the various lithofacies, suggests that the limestones and shales were deposited from an essentially iron-depleted shallow surface water mass close to shore in areas of high organic productivity and minor siliciclastic input; in contrast, the iron-formations were deposited in an iron-enriched deeper ocean water mass removed from high organic productivity and any terrigenous detritus.

The cross plots of organic carbon versus δ_{ca} (Fig. 7a) and total iron (Fig. 9) strongly support such an interpretation because they clearly define two different trends for the rock assemblage limestone-shale on the one hand and iron-formation on the other. These can be explained by deposition from two different water masses: (1) a nearshore shallow water mass with a carbon isotope composition enriched in ^{13}C and providing the source for the lighter carbonate carbon of the limestones and shales, and (2) an offshore, deeper water mass depleted in ^{13}C producing the siderite-rich iron-formations.

This concept is well illustrated by a cross plot of organic carbon and Al_2O_3 showing an excellent positive correlation between these two variables (Fig. 12a). It illustrates that limestone and shale deposition had much more in common than iron-formation and shale deposition (Fig. 12a) even though the latter two often constitute distinct stratigraphic assemblages (Fig. 2). This diagram also allows for a better understanding of the carbon isotope signature of the oxide-rich iron-formations. It illustrates that the oxide-rich iron-formations may initially have contained as much carbon as the siderite-rich iron-formations but that part of the carbon was removed (Fig. 12a) in the oxide facies by oxidation at the expense of Fe^{+3} (as part of inorganic reactions during diagenesis). A cross plot of Th versus organic carbon supports this consideration (Fig. 12b). The CO_2 so formed may have contributed to the depletion of ^{13}C in the carbonates from the oxide-rich iron-formations relative to those from the siderite-rich iron-formations. Petrographically it is evident that magnetite replaces hematite (Beukes, 1984) and such magnetite may be a product of this process as suggested by Perry et al. (1973). However, the relative loss of organic matter (0.068 wt %) may be too small to account for all the magnetite present in the iron-formations. Other ways of forming magnetite are through reduction of hematite by ferrous iron (Ewers and Morris, 1981) or oxidation of siderite (Beukes, 1984; Kaufman et al., 1990) which could account for additional euhedral magnetite. In contrast, anhedral fine-grained magnetite may represent a primary precipitate (Klein, 1974).

Source of light carbonate carbon in siderite-rich iron-formation

The question now to be asked is what is the origin of the ^{13}C-depleted carbonate carbon signature in the siderite-rich iron-formations? Does it reflect a primary source or is it the result of organic carbon oxidation? There are two aspects to this problem: (1) what is the origin of ^{13}C-depleted carbon in early Proterozoic deep ocean water? and (2) what other processes may have led to further depletion of the iron-formation carbonates?

In models by Cloud (1973), Walker (1984, 1987), and Baur et al. (1985), which assume essentially anoxygenous atmospheric conditions during the early Precambrian and relate iron-formation deposition to biologic production of O_2, light carbonate carbon in iron-formation is derived from oxidation of organic matter. A problem with such models, however, is that the abundance of reduced organic matter required for oxidation and subsequent incorporation into ^{13}C-depleted carbonates is not preserved in the iron-formations and probably was not there originally, possibly having been transported elsewhere (Cloud, 1973; Walker, 1987). Very relevant input into this problem is provided by Klein and Beukes (1989) who point out that, in the case of the Campbellrand-Kuruman transition sequence, high organic productivity was related to deposition of the stromatolitic carbonates and associated shale units, but that during deposition of the iron-formation organic productivity in the water column above it may have been relatively low. Such a concept is supported by the fact that Ba shows a good correlation with organic carbon contents in the sequence (Fig. 12c) and is depleted in the iron-formations relative to the limestones and shales. In modern ocean systems Ba in sediments is positively correlated with areas of high organic productivity (Dymond, 1985; Schmitz, 1987; Bishop, 1988) which,

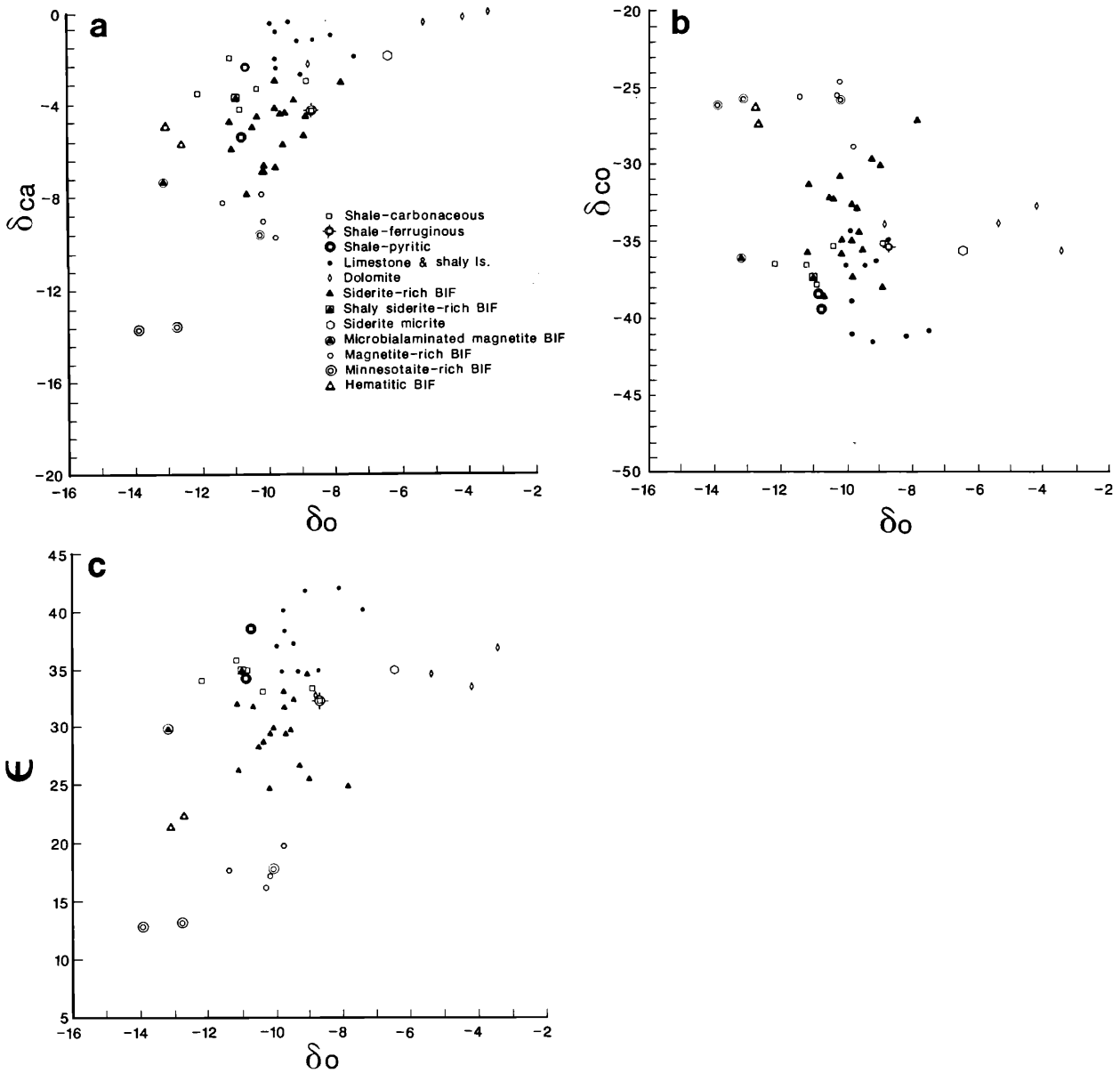

FIG. 10. Plots of oxygen versus carbon isotopes.

with reference to Figure 12b, would imply low productivity in the water column above the iron-formations.

In addition to questions about productivity it is also important to consider exactly where in the water column siderite may have precipitated. Kerogen-stained siderite in microbialaminated units may well have formed at the sediment-water interface making use of organic matter as a nucleus. Exactly the same mechanism may have been involved in the formation of the kerogenous calcmicrosparites in the microbialaminated limestones. Clastic-textured siderite mesobands provide no answer as to where siderite precipitated but they do illustrate that reworked siderite particles could be transported near the basin floor without being altered. Such types of siderite mesobands are, however, minor relative to those displaying fine regular laminations and which could have formed from settling of suspended siderite precipitate out of the water column. Such a process would also apply to the evenly banded siderite microbands that grade into chert microbands with dispersed siderite particles. This type of microbanding is very similar to that in deep-water evaporites as in the Castile Formation,

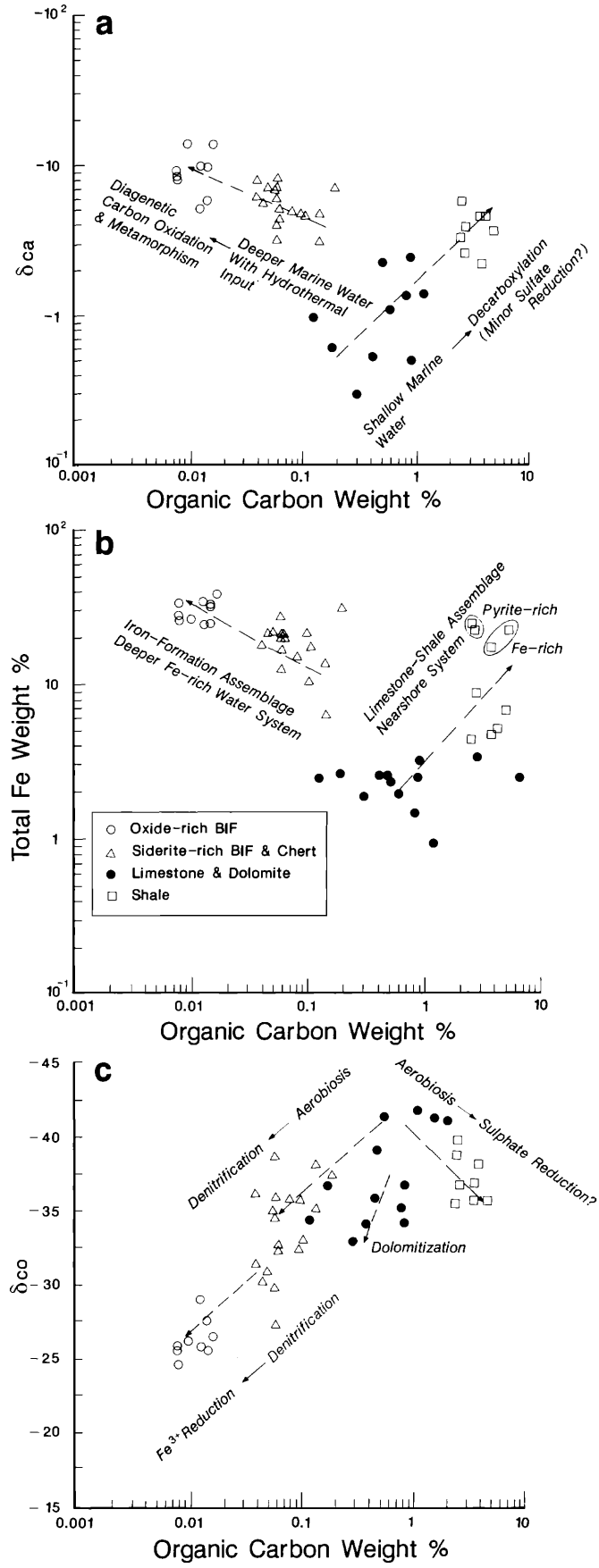

FIG. 11. Interpretation of various conditions at the time of origin of the lithofacies on the basis of total organic carbon versus carbon isotopes and total Fe (expressed as FeO).

TABLE 6. Isotopic Composition of Microdrilled Carbonate Samples from the Gamohaan Formation, Danielskuil

Sample no.	Description	δ_{ca}[1]	δ_o[2]
28-1-J	Micrite	+0.06	−8.14
	Sparite	+0.78	−6.80
28-1-X	Micrite	+1.07	−6.83
	Sparite	+0.10	−9.05
28-1-K	Micrite	−0.04	−7.24
28-1-C	Micrite	+0.00	−7.57

[1] δ_{ca} = carbonate carbon
[2] δ_o = carbonate oxygen

a feature also noted by Garrels (1987). Here microbands composed of calcite grains may alternate with anhydrite microbands containing dispersed calcite grains. Sedimentation models for this type of microbanding favor ideas of the different components having formed from seasonal fluctuations in relatively shallow water of the depository and having subsequently settled to the bottom (Schmalz, 1969; Dean et al., 1975). Similarly, siderite microsparite in the iron-formations may have been formed along a chemocline in the water column and subsequently have settled to the bottom.

It is therefore considered unlikely that the light isotopic signature in the carbonates from the iron-formations (Fig. 11a), and especially that of the siderite-rich units, could have been derived exclusively from organically derived CO_2 mixed with normal marine water having a $\delta^{13}C$ composition of about zero. The reason for this is that there may just not have been enough organic matter in the depositional environment of the siderite-rich iron-formations. Instead the light carbon may have a hydrothermal origin because hydrothermal water circulating through older organic-rich sediments may be depleted by as much as −15 to −20 per mil in ^{13}C (A. Ijima, pers. commun., 1988). Also Klein and Beukes (1989) note a distinct hydrothermal signature for the REE and trace element compositions of the deeper ocean water layer from which the iron-formations were deposited. The light isotopic signature may also have been derived from a mixture of hydrothermal, volcanic, and mantle-derived carbon. The average $\delta^{13}C$ composition of volcanic or mantle carbon is −6 per mil (Perry et al., 1973; Des Marais and Moore, 1984). The overall range for volcanic or mantle carbon is −3 to −8 per mil in carbonates (Taylor et al., 1967; Deines, 1970) to as light as −8 to −12 per mil in volcanic gases (Craig, 1963). If the total dissolved CO_2 in bottom water and hence marine phreatic water already had a light carbonate signature, subsequent addition of organically derived light CO_2 during diagenesis could have led to formation of additionally depleted sparry ankerites and/or ferroan dolomites with $\delta^{13}C$ values of −10 to −13 per mil.

The ^{18}O isotope composition of the carbonates from limestones and iron-formations also suggests a hydrothermal source for a portion of the isotopic depletion in carbonate carbon. The limestones and iron-formations are depleted in ^{18}O by 7 to 12 per mil relative to modern carbonates. This depletion is comparable to that observed in modern submarine hydrothermal water from which ^{18}O has been extracted through seafloor alteration of volcanics (Lawrence et al., 1976). The ancient water column may also have been stratified with regard to ^{18}O composition. Theoretically, siderite should be enriched by about 1 per mil in ^{18}O relative to calcite at 25°C (Golyshev et al., 1981; Kaufman et al., in press), but, among these samples the siderite iron-formations are on average depleted in ^{18}O by 0.7 per mil relative to the limestones (Table 5). If isotopic equilibrium was attained during precipitation of carbonates, this implies a deeper water mass depleted in ^{18}O by about 1.7 per mil relative to surface water.

Although it is suggested that much of the siderite formed in the water column or at the sediment-water interface, it is not implied that all siderite in iron-formations formed in this manner. Certainly there are excellent examples in the Kuruman Iron Formation of early- and late-stage sparry siderites commonly with zoned grains (Van Wyk, 1987). Also some microsparites have an ankeritic composition (Van Wyk, 1987). The chemical composition of the carbonate minerals in iron-formations therefore is not diagnostic of their origin in a depositional to diagenetic sequence; rather it is their morphology and paragenetic relationships with other components that is diagnostic.

Kerogen carbon isotope composition

According to the stratified ocean model for the deposition of the Campbellrand-Kuruman transition zone developed by Klein and Beukes (1989) the highest primary productivity occurred in the photic zone in association with benthic microbial mats forming limestones. This organic matter, part of which was transported to areas of shale deposition, was most depleted in ^{13}C with respect to other lithofacies with an average δ_{co} value of −37.5 per mil in limestone and −36.6 per mil in shale. The slightly heavier nature of the organic carbon in the shales may be ascribed to more effective sulfate reduction in them relative to that in limestone (Fig. 11c). The high variability of δ_s values in the sequence (Table 5) suggests that sulphate-reducing bacteria were active. Some samples are very much enriched in ^{34}S which would suggest closed-system reduction (Cameron, 1982).

There is a close link between the carbon isotope composition of the organic matter in the siderite-rich

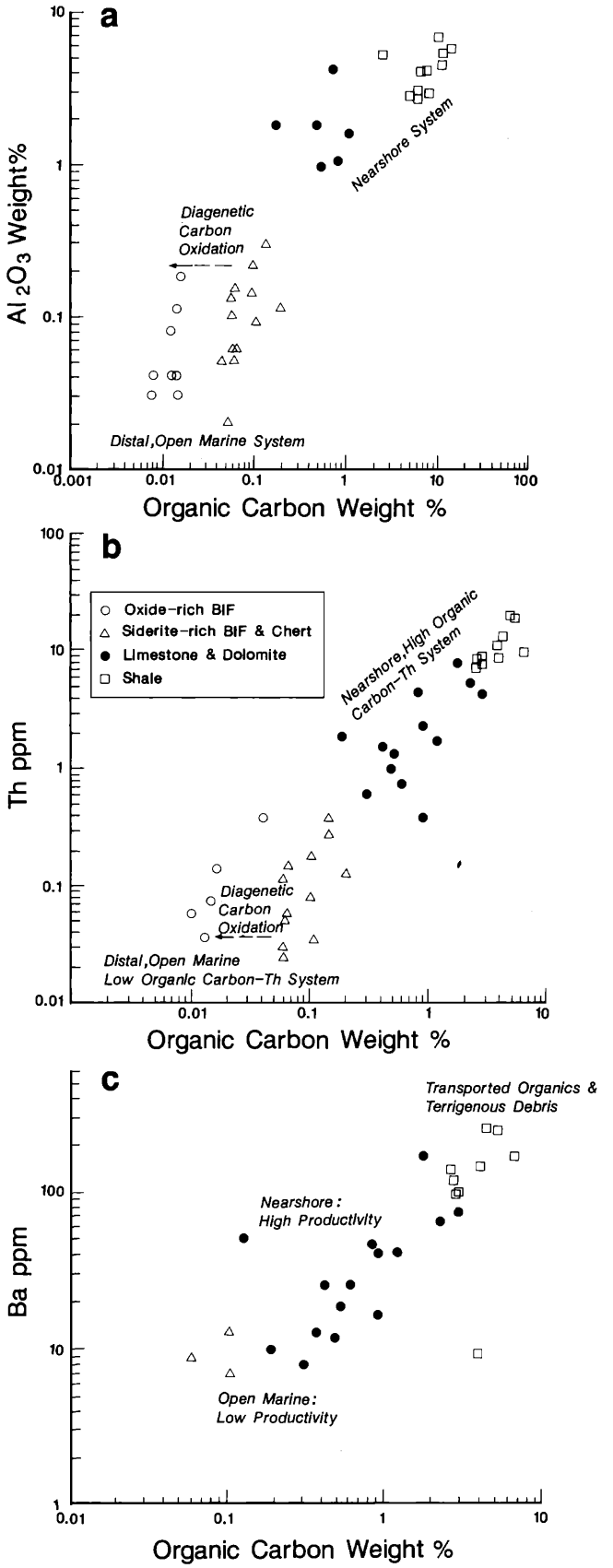

FIG. 12. Interpretation of various conditions at the time of origin of the lithofacies on the basis of total organic carbon versus Al_2O_3 (from Klein and Beukes, 1989), Th, and Ba.

iron-formations and that in the limestones and shales (Fig. 11c). On average, the organic matter in the siderite-rich iron-formations is, however, somewhat enriched in ^{13}C over that of the limestones and shales (Fig. 5) suggesting that it underwent a higher degree of degradation. The shallow surface water in the Campbellrand-Kuruman basin may have been somewhat oxygenated (Klein and Beukes, 1989) such that it must be assumed that any organic matter settling through the water column was subject to oxidation. Siderite is, however, only stable under strongly reducing conditions in the virtual absence of sulfide (Berner, 1971; Klein and Bricker, 1977). The supply of organics to the place of formation of the siderites could not have been large enough to sustain bacterial sulfate reduction, otherwise pyrite would have been precipitated in place of siderite. Oxidation of organic matter by ferric iron is known to precede sulfate reduction and to follow denitrification in the diagenetic environment (Froelich et al., 1979; Jørgenson, 1983). However, oxidation of organic matter by ferric iron was apparently most effective in the oxide-rich iron-formations leaving behind the smallest and isotopically heaviest kerogen residue of all lithofacies (Fig. 11c). It is thus suggested that the siderites were deposited in an environment where oxidation of organic matter occurred, if at all, by denitrification (Fig. 11c). The combination of aerobic oxidation and denitrification thus most probably resulted in the slightly heavier kerogen residue in the siderite-rich iron-formations relative to that in the limestones (Fig. 11c).

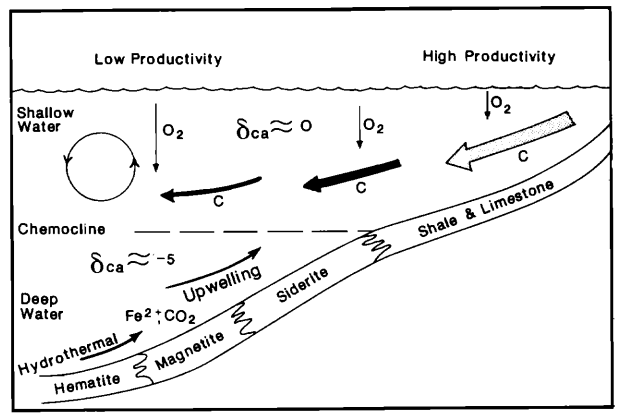

FIG. 13. Schematic depositional environment for the iron-formation and associated lithofacies in a marine system with a stratified water column. The thick arrows labeled C (organic carbon) represent high productivity whereas thinner arrows represent lesser carbon productivity and supply. Siderite precipitates along the chemocline where the organic carbon supply is such that reducing conditions prevail, and magnetite and hematite where the organic matter supply is so low that oxidizing conditions pertain. Regions where such materials accumulate may not necessarily be related to differences in depth. See text for discussion of the various isotopic values shown.

Conclusions

A major conclusion derived from the study of the transition zone between the Campbellrand carbonates and the Kuruman Iron Formation is that the carbonates and the kerogen components have undergone complex diagenetic alterations in all the lithofacies, that is, limestone, dolomite, shale, and the iron-formations including siderite-, magnetite-, hematite-, and minnesotaite-rich varieties. Recognition of these alterations as well as careful chemostratigraphic analysis are crucial to understanding the whole-rock carbon and oxygen isotope signatures in the sequence. Especially important to this study is the understanding of the formation of abundant late diagenetic, postcompactional sparry carbonates in the iron-formations and shales. They may have formed during a period of thermal decarboxylation and hence are more depleted in ^{13}C than the associated earlier carbonates. Contact metamorphism caused by a diabase sill enhanced ^{13}C depletion in the carbonates of the close-by iron-formations mainly through reaction of isotopically heavier siderite to form minnesotaite in the presence of quartz. The remaining ferroan dolomite and ankerite are significantly depleted in ^{18}O relative to unmetamorphosed rocks. In contrast, dolomitization of the limestones resulted in enrichment of ^{18}O ascribed to normal mineralogic fractionation between calcite and dolomite. Low-grade metamorphic minnesotaite-bearing iron-formation samples have ϵ values as low as 12.8 to 13.2 per mil which is about 4 to 20 per mil less than those from unmetamorphosed units (Tables 3 and 4).

Deep burial diagenesis, accompanied by sutured and nonsutured seam solution, led to the recrystallization of carbonates and exsolution of kerogen pigmentation from early diagenetic and primary carbonates represented by calcmicrosparite in limestones and siderite microsparite in iron-formations. Because this is merely a recrystallization process, it probably had very little effect on the overall isotopic composition of the lithofacies involved.

Probably the most significant conclusion of this paper is that taking all possible postdepositional effects on carbonate carbon isotope composition into consideration, there remains a primary difference in the isotopic signature of calcmicrosparite in limestone (δ_{ca} on average slightly negative at $-1.3‰$) and siderite microsparite in iron-formation (δ_{ca} on average markedly negative at $-5.3‰$). Because these minerals formed contemporaneously in the same basin, with limestone in shallow water and iron-formation in deeper water, it necessitates a water column stratified with regard to the isotopic composition of total dissolved CO_2 (i.e., a ^{13}C-depleted deeper water mass). A stratified water system for deposition of the transition sequence has been suggested by Klein and

Beukes (1989) on the basis of geochemical (especially trace and rare earth element compositions of the various lithofacies) and sedimentologic parameters. According to this model (simplified here to relate it to our isotopic information, Fig. 13) stromatolitic carbonates associated with high organic carbon productivity were deposited close to shore with iron-formation deposited distally in areas of low productivity and little influx of organic matter and terrigenous detritus (shale). Low supplies of organics to the area of iron-formation deposition exclude the possibility that the light carbon signature in the siderites was derived solely from degraded organic matter.

It is therefore suggested that the stratification in the basin water with respect to the isotopic composition of total dissolved CO_2 was related to a significant hydrothermal input (Fig. 13). In contrast, total dissolved CO_2 in the shallow, well-mixed and near-shore water masses, where limestone deposition took place, had a ^{13}C carbonate composition similar to that of present-day oceans, close to zero. Basin water was also depleted in δ_o relative to modern marine water by about 10 per mil possibly due to the hydrothermal input. REE and other trace element results presented by Klein and Beukes (1989) strongly support such a hydrothermal signature.

In this model the productivity of oxygen-producing photosynthesizers and the deposition of iron-formation are clearly decoupled. An important implication of this is that some oxygen must have been available in the shallow water of the basin to account for deposition of oxide facies iron-formation in the deeper part of the basin. This would suggest the presence of some oxygen in the atmosphere and surface ocean at that time.

The deeper basin system must have been reducing to allow for transportation of ferrous iron in solution, which upon mixing with somewhat oxygenated shallow water along a chemocline precipitated oxide-containing iron-formations. The amounts of oxygen available along the chemocline were dependent upon the supply of organic matter from nearshore areas and the photic zone. In areas of increased supply of organic matter, conditions along the chemocline may have been reducing and siderite could have precipitated. In more open-water areas, with the organic flux lower than that of oxygen and somewhat oxygenated conditions along the chemocline, insoluble ferric oxyhydroxide complexes and hence oxide-rich iron-formations formed. Minor amounts of organic matter that settled with the ferric iron components were further oxidized to produce a sediment extremely depleted in organic carbon. Because of this high level of degradation, the kerogen in oxide-rich iron-formation is also most enriched in ^{13}C relative to that in all other facies. In contrast, siderite-rich iron-formations were deposited in areas where organic matter was decomposed mainly by denitrification following initial aerobic oxidation. This organic matter is thus less depleted in ^{13}C than that of the oxide-rich iron-formations. Benthic microbial organisms associated with limestone deposition may have been the source of much of the organic matter preserved even in the iron-formations.

The stratified basin water model cannot be easily ascribed to a signal specific to the Campbellrand-Kuruman depositional event. Too many arguments, summarized by Klein and Beukes (1989), favor a rather open-marine system during deposition; as would the carbonate carbon isotope composition of the limestones presented here. Iron-formation deposition was specifically coupled to a major transgressive event (Beukes, 1984, 1987; Klein and Beukes, 1989) which would imply even more open-marine conditions. The only difference with a true ocean system is that deposition took place on a very extensive submerged platform, most probably facing a back-arc basin, in relatively shallow water. Water depths for deposition of the microbanded iron-formation must have been on the order of 100 to 700 m (Klein et al., 1987) with the extent of the submerged platform exceeding 600,000 km^2 (Beukes, 1987). This makes derivation of reduced iron species from a local source most unlikely and may suggest a connection between reducing deeper water on the platform and/or back-arc basin with that of the true open ocean. Restriction of circulation is, however, inherent in such an extensive shallow sea system and may have contributed toward deposition of the iron-formation, especially the silica component through enhanced salinity.

A connection between the deeper water of the basin and that of the open ocean may imply that the ocean system 2.3 to 2.5 b.y. ago was also stratified with regard to the ^{13}C composition of total dissolved carbon in contrast with present-day oceans (Schidlowski et al., 1983). In this regard it is important to note that ^{13}C depletion in carbonates from iron-formations relative to that of limestones and dolomites appears to be the norm in the early Precambrian (Becker and Clayton, 1972; Perry and Tan, 1972; Perry et al., 1973; Perry and Ahmad, 1981; Goodwin et al., 1985; Baur et al., 1985; Kaufman et al., in press). The concept of an ocean stratified with regard to carbon isotopes should be further tested through isotopic studies in which deep and shallow marine lithofacies are carefully distinguished, and for which paragenetic sequences in carbonate mineral assemblages and kerogen distributions are well established.

Acknowledgments

We thank the management and geologic staff of the Griqualand Exploration and Finance Company, Kuruman, South Africa, for giving us access to the

three diamond drill cores that form the basis for this study. N.J.B. acknowledges Rand Afrikaans University and the Foundation for Research Development, Council for Scientific and Industrial Research, for several research allocations and support during a sabbatical leave in 1987–1988. We thank Joy A. Beier of Indiana University for the isotopic analyses of several microdrilled samples (Table 6) and Ján Veizer for the sulfur isotope determinations. We acknowledge Sharon Fisher for very careful and patient typing and retyping of various manuscript versions and Dag Lopez for the drafting of the illustrations. We are grateful to J. W. Schopf of University of California, Los Angeles, and the Center for the Study of Evolution and the Origin of Life (CSEOL) for support during our respective research leaves in 1987–1988. This research was made possible by National Science Foundation grants EAR-8419161, EAR-845681, and EAR-8617805 to C.K. and NASA grant NGR 15003-118 to J.M.H.

June 5, 1989; March 5, 1990

REFERENCES

Baur, M. E., Hayes, J. M., Studley, S. A., and Walter, M. R., 1985, Millimeter-scale variations of stable isotope abundances in carbonates from banded iron-formations in the Hamersley Group of Western Australia: ECON. GEOL., v. 80, p. 270–282.

Becker, R. H., and Clayton, R. N., 1972, Carbon isotopic evidence for the origin of a banded iron-formation in Western Australia: Geochim. et Cosmochim. Acta, v. 36, p. 577–595.

Berner, R. A., 1971, Principles of chemical sedimentology: New York, McGraw-Hill, 229 p.

—— 1981, A new geochemical classification of sedimentary environments: Jour. Sed. Petrology, v. 51, p. 359–365.

Beukes, N. J., 1983, Palaeoenvironmental setting of iron-formations in the depositional basin of the Transvaal Supergroup, South Africa, *in* Trendall, A. F., and Morris, R. C., eds., Iron-formations: Facts and problems: Amsterdam, Elsevier, p. 131–209.

—— 1984, Sedimentology of the Kuruman and Griquatown iron-formations, Transvaal Supergroup, Griqualand West, South Africa: Precambrian Research, v. 245, p. 47–84.

—— 1987, Facies relations, depositional environments and diagenesis in a major early Proterozoic stromatolitic carbonate platform to basinal sequence, Campbellrand Subgroup, Transvaal Supergroup, southern Africa: Sed. Geology, v. 54, p. 1–46.

Beukes, N. J., and Smit, C. A., 1987, New evidence for thrust faulting in Griqualand West, South Africa: Implications for stratigraphy and the age of red beds: South African Jour. Geology, v. 90, p. 378–394.

Bishop, J. K. B., 1988, The barite-opal-organic carbon association in oceanic particulate matter: Nature, v. 332, p. 341–343.

Button, A., 1976, Transvaal and Hamersley basins—review of basin development and mineral deposits: Minerals Sci. Eng., v. 8, p. 262–293.

Cameron, E. M., 1982, Sulphate and sulphate reduction in early Precambrian oceans: Nature, v. 296, p. 145–148.

Cloud, P., 1973, Paleoecological significance of the banded iron-formation: ECON. GEOL., v. 68, p. 1135–1143.

Coleman, M. L., 1985, Geochemistry of diagenetic non-silicate minerals: Kinetic considerations: Roy. Soc. [London] Philos. Trans., v. A315, p. 39–56.

Craig, H., 1963, The isotopic geochemistry of water and carbon in geothermal areas, *in* Tongiargi, E., ed., Nuclear geology in geothermal areas: Pisa, Consiglio Nazionale Richerche, p. 17–53.

Dean, W. E., Davies, G. R., and Anderson, R. Y., 1975, Sedimentological significance of nodular and laminated anhydrite: Geology, v. 3, p. 367–372.

Deines, P., 1970, The carbon and oxygen isotopic composition of carbonates from the Oka carbonate complex, Quebec, Canada: Geochim. et Cosmochim. Acta, v. 34, p. 1199–1225.

Des Marais, D. J., and Moore, J. G., 1984, Carbon and its isotopes in mid-oceanic basaltic glasses: Earth Planet. Sci. Letters, v. 69, p. 43–57.

Dymond, J., 1985, Particulate barium fluxes in the oceans: An indicator of new productivity [abs.]: Am. Geophys. Union Trans., v. 66, p. 1275.

Ewers, W. E., and Morris, R. C., 1981, Studies of the Dales Gorge Member of the Brockman Iron Formation, Western Australia: ECON. GEOL., v. 76, p. 1929–1953.

Fisher, A. G., Honjo, S., and Garrison, R. W., 1967, Electron micrographs of limestones and their nannofossils: Princeton, Princeton Univ. Press, 137 p.

Folk, R. L., 1974, The natural history of crystalline calcium carbonate: Effect of magnesium content and salinity: Jour. Sed. Petrology, v. 44, p. 40–53.

Froelich, P. N., Klinkhammer, G. P., Bender, M. L., Luedtke, N. A., Heath, G. R., Cullen, D., and Dauphin, P., 1979, Early oxidation of organic matter in pelagic sediments of the eastern Atlantic: Suboxic diagenesis: Geochim. et Cosmochim. Acta, v. 43, p. 1075–1090.

Garrels, R. M., 1987, A model for the deposition of the microbanded Precambrian iron-formations: Am. Jour. Sci., v. 187, p. 81–106.

Golyshev, S. I., Padalko, N. L., and Pechenkin, S. A., 1981, Fractionation of stable oxygen and carbon isotopes in carbonate systems: Geochemistry Internat., v. 18, p. 85–99.

Goodwin, A. M., Thode, H. G., Chou, C. L., and Karkhansis, S. N., 1985, Chemostratigraphy and origin of the late Archean siderite-pyrite-rich Helen Iron Formation, Michipicoten belt, Canada: Canadian Jour. Earth Sci., v. 22, p. 72–84.

Gregory, R. T., 1986, Oxygen isotope systematics of quartz-magnetite pairs from Precambrian iron formations: Evidence for fluid-rock interaction during diagenesis and metamorphism, *in* Walther, J. V., and Wood, B. J., eds., Fluid-rock interactions during metamorphism: New York, Springer-Verlag, p. 132–153.

Hoefs, J., 1987, Stable isotope geochemistry: Berlin, Springer-Verlag, 241 p.

Hoffman, P. F., 1987, Early Proterozoic foredeeps, foredeep magmatism, and Superior-type iron-formations of the Canadian Shield, *in* Kröner, A., ed., Proterozoic lithospheric evolution: Geodynamic series: Washington, Am. Geophys. Union, v. 17, p. 85–97.

Jørgenson, B. B., 1983, Processes at the sediment-water interface, *in* Bolin, B., and Cook, R. B., eds., The major biogeochemical cycles and their interactions: SCOPE, Rept. 21, Chichester, England, John Wiley, p. 477–515.

Kaufman, A. J., Hayes, J. M., and Klein, C., Mineralogic control of isotopic compositions in microbanded carbonates and cherts from a banded iron-formation: Geochim. et Cosmochim. Acta, in press.

Klein, C., 1974, Greenalite, stilpnomelane, minnesotaite, crocidolite and carbonates in a very low-grade metamorphic Precambrian iron-formation: Canadian Mineralogist, v. 12, p. 475–498.

Klein, C., and Beukes, N. J., 1989, Geochemistry and sedimentology of a facies transition from limestone to iron-formation deposition in the early Proterozoic Transvaal Supergroup, South Africa: ECON. GEOL., v. 84, p. 1733–1774.

Klein, C., Jr., and Bricker, O. P., 1977, Some aspects of the sedimentary and diagenetic environment of Proterozoic banded iron-formation: ECON. GEOL., v. 72, p. 1457–1470.

Klein, C., Beukes, N. J., and Schopf, J. W., 1987, Filamentous microfossils in the early Proterozoic Transvaal Supergroup: Their morphology, significance and paleoenvironmental setting: Precambrian Research, v. 36, p. 81–94.

Land, L. S., 1980, The isotopic and trace element geochemistry of dolomite: The state of the art: Soc. Econ. Paleontologists Mineralogists Spec. Pub., v. 28, p. 87–110.

Lawrence, J. R., Gieskes, J., and Anderson, T. F., 1976, Oxygen isotope materials balance calculations, leg 35: Deep Sea Drilling Proj., Initial Repts., v. 35, p. 505–512.

Miyano, T., and Beukes, N. J., 1984, Phase relations of stilpnomelane, ferriannite and riebeckite in very low-grade metamorphosed iron-formations: Geol. Soc. South Africa Trans., v. 87, p. 111–124.

Nel, C. J., Beukes, N. J., and DeVilliers, J. P. R., 1986, The Mamatwan manganese mine of the Kalahari manganese field, *in* Anhaeusser, C. R., and Maske, S., eds., Mineral deposits of southern Africa, vol. 1: Johannesburg, Geol. Soc. South Africa, p. 963–978.

Perry, E. C., Jr., and Ahmad, S. N., 1981, Oxygen and carbon isotope geochemistry of the Krivoy Rog iron formation, Ukranian SSR: Lithos, v. 14, p. 83–92.

—— 1983, Oxygen isotope geochemistry of Proterozoic chemical sediments: Geol. Soc. America Mem., v. 161, p. 253–264.

Perry, E. C., Jr., and Tan, F. C., 1972, Significance of oxygen and carbon isotope variations in early Precambrian cherts and carbonate rocks of southern Africa: Geol. Soc. America Bull., v. 83, p. 647–664.

Perry, E. C., Jr., Tan, F. C., and Morey, G. B., 1973, Geology and stable isotope geochemistry of the Biwabik Iron-Formation, northern Minnesota: ECON. GEOL., v. 68, p. 1110–1125.

Rosenbaum, J., and Sheppard, S. M. F., 1986, An isotopic study of siderites, dolomites, and ankerites at high temperatures: Geochim. et Cosmochim. Acta, v. 50, p. 1147–1150.

Sasaki, A., Arikawa, Y., and Folinsbee, R. A., 1979, Kiba reagent method of sulfur extraction applied to isotopic work: Japan Geol. Survey Bull., v. 30, p. 241–245.

Schidlowski, M., Hayes, J. M., and Kaplan, I. R., 1983, Isotopic inferences of ancient biochemistries: Carbon, sulfur, hydrogen, and nitrogen, *in* Schopf, J. W., ed., Earth's earliest biosphere: Its origin and evolution: Princeton, Princeton Univ. Press, p. 149–186.

Schmalz, R. F., 1969, Deep-water evaporite deposition: A genetic model: Am. Assoc. Petroleum Geologists Bull., v. 53, p. 798–823.

Schmitz, R., 1987, Barium, equatorial high productivity, and the northward wandering of the Indian continent: Paleoceanography, v. 2, p. 63–77.

Stowe, C. W., 1986, Synthesis and interpretation of structures along the north-eastern boundary of the Namaqua tectonic province, South Africa: Geol. Soc. South Africa Trans., v. 89, p. 85–198.

Taylor, H. P., Frechen, J., and Degens, E. T., 1967, Oxygen and carbon isotope studies of carbonates from the Laacher See district, West Germany and the Alno district, Sweden: Geochim. et Cosmochim. Acta, v. 31, p. 407–430.

Van Wyk, C. J., 1987, Die mineralogie en geochemie van sedimentere siklusse in die Kuruman en Griquatown-Ysterformasies van die Transvaal-Supergroep in Griekwaland-Wes: Unpub. M.Sc. thesis, Johannesburg, Rand Afrikaans Univ., 235 p.

Wachter, E. A., and Hayes, J. M., 1985, Exchange of oxygen isotopes in carbon dioxide-phosphoric acid systems: Chem. Geology, v. 52, p. 365–374.

Walker, J. C. G., 1984, Suboxic diagenesis in banded iron formations: Nature, v. 309, p. 340–342.

—— 1987, Was the Archaean biosphere upside down?: Nature, v. 329, p. 710–712.

Walraven, F., Armstrong, R. A., and Kruger, F. J., 1990, A chronostratigraphic framework for the north-central Kaapvaal craton, the Bushveld Complex and the Vredefort structure: Tectonophysics, v. 171, p. 23–48.